



**UNIVERSITY OF LEEDS**

This is a repository copy of *AQP5 enriches for stem cells and cancer origins in the distal stomach*.

White Rose Research Online URL for this paper:  
<http://eprints.whiterose.ac.uk/155846/>

Version: Accepted Version

---

**Article:**

Tan, SH, Swathi, Y, Tan, S et al. (21 more authors) (2020) AQP5 enriches for stem cells and cancer origins in the distal stomach. *Nature*, 578 (7795). pp. 437-443. ISSN 0028-0836

<https://doi.org/10.1038/s41586-020-1973-x>

---

© 2020, Springer Nature . This is an author produced version of a paper published in *Nature*. Uploaded in accordance with the publisher's self-archiving policy.

**Reuse**

Items deposited in White Rose Research Online are protected by copyright, with all rights reserved unless indicated otherwise. They may be downloaded and/or printed for private study, or other acts as permitted by national copyright laws. The publisher or other rights holders may allow further reproduction and re-use of the full text version. This is indicated by the licence information on the White Rose Research Online record for the item.

**Takedown**

If you consider content in White Rose Research Online to be in breach of UK law, please notify us by emailing [eprints@whiterose.ac.uk](mailto:eprints@whiterose.ac.uk) including the URL of the record and the reason for the withdrawal request.



[eprints@whiterose.ac.uk](mailto:eprints@whiterose.ac.uk)  
<https://eprints.whiterose.ac.uk/>

1 **AQP5 Enriches for Stem Cells and Cancer Origins in the Distal Stomach**

2 Si Hui Tan<sup>1§</sup>, Yada Swathi<sup>1§</sup>, Shawna Tan<sup>1</sup>, Jasmine Goh<sup>1</sup>, Ryo Seishima<sup>1</sup>, Kazuhiro  
3 Murakami<sup>2</sup>, Masanobu Oshima<sup>3</sup>, Toshikatsu Tsuji<sup>4</sup>, Phyllis Phuah<sup>1</sup>, Liang Thing Tan<sup>1</sup>, Esther  
4 Wong<sup>1</sup>, Aliya Fatehullah<sup>1</sup>, Taotao Sheng<sup>5,6</sup>, Shamaine Wei Ting Ho<sup>5,7</sup>, Heike Grabsch<sup>8,9</sup>,  
5 Supriya Srivastava<sup>10,11</sup>, Ming Teh<sup>10</sup>, Simon L.I.J. Denil<sup>12</sup>, Seri Mustafah<sup>13</sup>, Patrick Tan<sup>5</sup>, Asim  
6 Shabbir<sup>14</sup>, Jimmy So<sup>14</sup>, Khay Guan Yeoh<sup>11</sup>, and Nick Barker<sup>1, 2, 15, \*</sup>

7

8 <sup>1</sup> A\*STAR Institute of Medical Biology, Singapore, 138648 Singapore

9 <sup>2</sup> Division of Epithelial Stem Cell Biology, Cancer Research Institute, Kanazawa University,  
10 Kakuma-machi Kanazawa, 920-1192, Japan

11 <sup>3</sup> Division of Genetics, Cancer Research Institute, Nano-Life Science Institute, Kanazawa  
12 University, Kakuma-machi, Kanazawa 920-1192, Japan

13 <sup>4</sup> Department of Gastroenterological Surgery, Ishikawa Prefectural Central Hospital,  
14 Kuratsuki-Higashi 2-1, Kanazawa 920-8530, Japan

15 <sup>5</sup> Cancer and Stem Cell Biology Program, Duke-NUS Graduate Medical School, Singapore,  
16 169857 Singapore

17 <sup>6</sup> Department of Biochemistry, National University of Singapore, Singapore, 117596 Singapore

18 <sup>7</sup> Cancer Science Institute of Singapore, National University of Singapore, Singapore, 117599  
19 Singapore

20 <sup>8</sup> Department of Pathology, GROW School for Oncology and Developmental Biology,  
21 Maastricht University Medical Center+, Maastricht, NL

22 <sup>9</sup> Pathology and Data Analytics, Leeds Institute of Medical Research at St. James's, University  
23 of Leeds, Leeds, UK

24 <sup>10</sup> Department of Pathology, National University Health System, Singapore, 119228 Singapore

25 <sup>11</sup> Department of Medicine, National University Health System, Singapore, 119228 Singapore

26 <sup>12</sup> Skin Research Institute of Singapore, Singapore 138648 Singapore

27 <sup>13</sup> A\*STAR Singapore Immunology Network, Singapore, 138648 Singapore

28 <sup>14</sup> Department of Surgery, National University Health System, Singapore, 119228 Singapore

29 <sup>15</sup> School of Biological Sciences, Nanyang Technological University, Singapore, 308232

30 Singapore

31 <sup>§</sup> Equal Contribution

32 \* Corresponding author

33 **Running title: AQP5 Enriches Stem Cells in Distal Stomach**

34

35

36 **Lgr5 marks resident adult epithelial stem cells at the gland base in the mouse pyloric**  
37 **stomach<sup>1</sup>, but the identity of the equivalent human stem cell population remains elusive**  
38 **due to a lack of surface markers facilitating its prospective isolation and validation.**  
39 **Lgr5+ intestinal stem cells are major sources of cancer following Wnt pathway**  
40 **hyperactivation in mice<sup>2</sup>. However, the contribution of pyloric Lgr5+ stem cells to**  
41 **gastric cancer following Wnt pathway dysregulation, a frequent event in human gastric**  
42 **cancer<sup>3</sup>, is unknown. Here, we employed comparative profiling of Lgr5+ stem cell**  
43 **populations along the mouse gastrointestinal tract to identify, then functionally validate**  
44 **the membrane protein AQP5 as a marker that enriches for mouse and human adult**  
45 **pyloric stem cells. We show that stem cells within the Aqp5+ compartment are a source**  
46 **of Wnt-driven, invasive gastric cancer *in vivo* using new *Aqp5-CreERT2* mouse models.**  
47 **Additionally, tumour-resident Aqp5+ cells can selectively initiate organoid growth *in***  
48 ***vitro*, indicating that this population harbours potential cancer stem cells. In human**  
49 **gastric cancer, AQP5 is robustly expressed in primary and metastases of intestinal and**  
50 **diffuse subtypes, often displaying altered cellular localization compared to healthy**  
51 **tissue. These new markers and mouse models will be an invaluable resource for**  
52 **deciphering early gastric cancer formation and for isolating and characterizing human**  
53 **stomach stem cells as a prerequisite to potentially harnessing their regenerative**  
54 **medicine potential in the clinic.**

### 55 **Comparative profiling yields new markers**

56 To identify markers specific to Lgr5<sup>Hi</sup> pyloric stem cells within the gastrointestinal tract, we  
57 profiled the transcriptomes of qPCR-validated Lgr5-EGFP<sup>Hi</sup> (Lgr5+ stem cells), Lgr5-EGFP<sup>Lo</sup>  
58 (immediate progeny) and unfractionated populations from the small intestine, colon, gastric  
59 pylorus of Lgr5-EGFP-IRES-CreERT2 mice<sup>4</sup> by microarray, and identified genes selectively  
60 enriched in Lgr5<sup>Hi</sup> pyloric stem cells (Fig. 1a; Extended Data Fig. 1a-d, Supplementary Table  
61 1). This dataset also revealed the transcriptional signature of Lgr5<sup>Hi</sup> colon stem cells  
62 (Supplementary Table 2). Profiling of Lgr5-EGFP<sup>Hi</sup>, Lgr5-EGFP<sup>Lo</sup> and Lgr5-EGFP<sup>Neg</sup> pylorus

63 populations from another *Lgr5*-reporter model, *Lgr5*-DTR-EGFP<sup>5</sup>, revealed 67 overlapping  
64 genes (Fig. 1b).

65 Candidate markers were empirically validated by qPCR, *in situ* hybridization (ISH) and  
66 immunostaining. Optimal candidates presented enriched expression in the *Lgr5*-EGFP<sup>Hi</sup>  
67 pyloric population by qPCR, robust, localized mRNA/protein expression within the *Lgr5*+  
68 pyloric gland base<sup>1</sup>, minimal expression in intestines and gastric corpus and co-expression  
69 with *Lgr5* (Extended Data Fig. 1j-n). Six candidates were selected: Alpha-1,4-N-  
70 Acetylglucosaminyltransferase (*A4gnt*), Aquaporin-5 (*Aqp5*), Gastric intrinsic factor (*Gif*),  
71 Mucin6 (*Muc6*), Solute carrier protein 9a3 (*Slc9a3/Nhe3*) and Secreted phosphoprotein 1  
72 (*Spp1/Osteopontin*) (Fig. 1c-m; Extended Data Fig. 1e-n, Supplementary Table 3).

73 To validate the six candidates as markers of pyloric stem cell-enriched populations, we  
74 generated EGFP-IRES-CreERT2 mouse models for *Aqp5*, *A4gnt*, *Spp1* and *Slc9A3*  
75 (Extended Data Fig. 2a), and *Aqp5*-2A-EGFP, *Slc9A3*-2A-EGFP, *Aqp*-2A-CreERT2 and  
76 *Slc9A3*-2A-CreERT2 mice in which endogenous gene expression is unaffected (Extended  
77 Data Fig. 2b). GFP expression in the pylori of the 2A-EGFP models recapitulated endogenous  
78 gene expression in the pylorus and small intestine (Extended Data Fig. 2c-f). Additionally,  
79 97.4% concurrence between the *Aqp5*+ and *Slc9a3*+ pyloric populations by co-staining  
80 (Extended Data Fig. 2g-h) reaffirms that they effectively label the same population.

81 The *in vivo* contribution of the gland populations expressing the candidate genes to epithelial  
82 renewal was evaluated via lineage tracing in CreERT2;*Rosa26*-tdTomato<sup>LSL</sup> lines. tdTomato  
83 (dTom) expression was first observed at the gland bases in all lines 20-48 hours post-  
84 Tamoxifen induction, confirming the expected Cre expression domain (Extended Data Fig. 3a-  
85 d, q-r). After several months (tissue turnover spans 7-10 days<sup>1</sup>), multiple entirely dTom+  
86 glands were evident throughout the pylorus, documenting the long-term self-renewal and  
87 multipotency of the cells expressing *Aqp5*, *Slc9A3*, *Spp1* or *A4gnt* (Extended Data Fig. 3e-h,  
88 s-t). Importantly, no intestinal tracing was observed, except for transient reporter expression

89 within the villi of *Slc9A3*-Cre models (Extended Data Fig. 2f, 3i-x). These observations confirm  
90 that populations expressing *Aqp5*, *Spp1*, *Slc9a3* and *A4gnt* contain pyloric stem cells.

91

## 92 **Aqp5 enriches for stem cells in mice**

93 *Aqp5* water channel protein<sup>6</sup> emerged as a promising candidate for isolating pyloric stem cells  
94 from mice and humans. EGFP expression was restricted to pyloric gland bases in *Aqp5*-  
95 EGFP-IRES-CreERT2 and *Aqp5*-2A-EGFP mouse models (Extended Data Fig. 2c,w). Sorted  
96 EGFP<sup>+</sup> cells from adult *Aqp5*-EGFP-IRES-CreERT2 mice (Fig. 2a) showed a 9-fold and 15-  
97 fold enrichment of *Aqp5* and *Lgr5* transcripts respectively over EGFP<sup>-</sup> cells (Extended Data  
98 Fig. 2u-v). By immunostaining, endogenous *Aqp5* protein co-localized with EGFP (Extended  
99 Data Fig. 2w). Thus, the *Aqp5* models faithfully report *Aqp5* expression in pyloric gland bases.

100 Next, we found that *Aqp5*<sup>+</sup> population overlapped with *Gif* and *Ki67* but not *Gastrin* (*Gast*),  
101 *Chromogranin A* (*Chga*) or *Mucin5ac* (*Muc5ac*), whilst the *Lgr5*-EGFP<sup>Hi</sup> population expressed  
102 major gastric lineage markers (*Gif*, *Gast*, *Chga*) and *Ki67* (Fig. 2b-e, Extended Data Fig. 2k-  
103 m, x). This observation was confirmed via single-cell analysis of *Lgr5*-EGFP<sup>Hi</sup> pyloric stem  
104 cells by CEL-Seq/RaceID<sup>7</sup>. The *Lgr5*-EGFP<sup>Hi</sup> compartment comprised three subpopulations:  
105 the major subpopulation co-expressed some of the new pyloric markers – *Aqp5*, *Gif* and *Muc6*  
106 (Extended Data Fig. 2n-q), while the two minor subpopulations expressed *Chga*/*Gast* and  
107 *Krt8*/*Krt18* (Extended Data Fig. 2r-s). Proliferation marker expression was significantly  
108 enriched in the major subpopulation (Extended Data Fig. 2t). *Aqp5* staining on *Lgr5*-DTR-  
109 EGFP pylori revealed 94.1% overlap between the two populations (Extended Data Fig. 2i-j),  
110 underscoring the CEL-Seq finding that *Aqp5* marks the major subpopulation of *Lgr5*<sup>Hi</sup> cells.

111 Lineage tracing using adult *Aqp5*-EGFP-IRES-CreERT2;*Rosa26*-tdTomato<sup>LSL</sup> (*Aqp5*-IRES-  
112 CreERT2;dTom) mice detailed the homeostatic behaviour of *Aqp5*<sup>+</sup> cells – dTom<sup>+</sup> cells  
113 appeared exclusively at the gland bases 20 hours post-tamoxifen induction (Fig. 2f, Extended  
114 Data Fig. 3y), expanded to clones reaching gland surfaces by 5 days (Fig. 2g), and persisted

115 for 1 year, demonstrating self-renewal of Aqp5+ cells (Fig. 2h-i, Extended Data Fig. 3z,c').  
116 Uninduced controls presented negligible dTom+ clones (Extended Data Fig. 3a'-b'). Six  
117 months post-induction, dTom+ clones comprised the major pyloric lineages expressing Gif,  
118 Gast, Chga and Muc5ac (Fig. 3j-m), confirming multipotency in the Aqp5+ population. Ablating  
119 endogenous Aqp5+ cells using a new Aqp5-2A-DTR model severely disrupted the gland  
120 bases (Extended Data Fig. 4k-r).

121 Tracing was absent from corpus, small intestine and colon, except for Brunner's glands  
122 (Extended Data Fig. 3d'-h'). Our Aqp5-2A-EGFP and Aqp5-CreERT2 models also faithfully  
123 reported endogenous Aqp5 expression in tissues such as cornea, lung, mammary gland and  
124 salivary gland<sup>13,14</sup> (data not shown).

125 To evaluate Aqp5's utility as a marker for isolating enriched pyloric stem cell populations, we  
126 sorted Aqp5+ and Aqp5- cells from adult wild-type mice using anti-Aqp5 antibody (Fig. 2n,  
127 Extended Data Fig. 4a-b) to profile their transcriptomes and evaluate their *in vitro* organoid-  
128 forming capacity. *Aqp5* and *Lgr5* were markedly enriched in Aqp5+ population relative to  
129 Aqp5- population by qPCR and microarray (Fig. 2o-p, Extended Data Fig. 4d-e). Aqp5+ and  
130 *Lgr5*-EGFP<sup>Hi</sup> transcriptomes are highly correlated by GSEA analysis (FDR p-value<0.001,  
131 Extended Data Fig. 4c), with the Aqp5+ population presenting strong enrichment of our new  
132 markers (Fig. 2q; Extended Data Fig. 4f) and published gland base markers, *Lrig1*<sup>8</sup> and  
133 *Runx1*<sup>9</sup> (Extended Data Fig. 4g). *Axin2*<sup>10</sup>, *Cck2r*<sup>11</sup> and *Sox2*<sup>12</sup> were not enriched in the Aqp5+  
134 population, consistent with their relatively broad expression within pyloric glands (Extended  
135 Data Fig. 4g). Concurring with immunostaining, Aqp5+ cells presented high *Gif*, moderate  
136 *Ki67* and no *Muc5ac* expression; there was no significant difference in *Gast* and *Chga*  
137 expression between Aqp5+ and Aqp5- populations, likely reflecting the limited numbers of  
138 Gastrin+ G cells and Chga+ endocrine cells within the Aqp5- population (Extended Data Fig.  
139 4h). Therefore, this antibody-based strategy facilitates enrichment of mouse pyloric stem cells,  
140 independent of fluorescent reporters.

141 Compared to Aqp5<sup>-</sup> cells, Aqp5<sup>+</sup> cells generated three-fold more organoids (0.64% vs 2.58%  
142 respectively) that could be maintained long-term, while the few organoids derived from Aqp5<sup>-</sup>  
143 cells died within 3 weeks (Fig. 2r-t). Organoid initiation frequencies from Aqp5<sup>+</sup> cells (2.58%)  
144 and Lgr5-EGFP<sup>+</sup> cells (3.09%) from Lgr5-2A-EGFP mice were similar (Extended Data Fig.  
145 4s-u), indicating high functional overlap. Aqp5<sup>+</sup> cell-derived organoids showed heterogeneous  
146 Aqp5 expression, which partially overlapped with Ki67 (Extended Data Fig. 4i-j), similar to its  
147 *in vivo* pattern. Withdrawal of WNT3A, FGF10 and NOGGIN (Fig. 2u) resulted in  
148 downregulation of stem cell markers *Lgr5*, *Aqp5* and upregulation of differentiation marker  
149 *Muc5ac* in the organoids after 3 days (Fig. 2v-x). Therefore, Aqp5 is a useful marker for the  
150 prospective isolation of enriched murine pyloric stem cells.

151

## 152 **AQP5 enriches for stem cells in humans**

153 We sought to evaluate AQP5 as a marker facilitating enrichment of human pyloric stem cells.  
154 AQP5 was exclusively expressed at human pyloric gland bases, overlapping with *LGR5* and  
155 other mouse pyloric markers, *MUC6*, *A4GNT* and *SLC9A3* (Fig. 3a-d, Extended Data Fig. 5a-  
156 f). A minor proportion of the human AQP5<sup>+</sup> cells were KI67<sup>+</sup> (Fig. 3e-f), reminiscent of the  
157 murine pylorus (Extended Data Fig. 2x). Human AQP5<sup>+</sup> cells overlapped with *PEPC*<sup>+</sup> and  
158 *MUC6*<sup>+</sup> populations, but, not *GIF*<sup>+</sup> parietal cells or *MUC5AC*<sup>+</sup> foveolar cells (Extended Data  
159 Fig. 5g-j).

160 We next sorted AQP5<sup>+</sup> cells from healthy human pyloric specimens using anti-AQP5 antibody  
161 and verified 10.2-fold enriched *AQP5* expression in AQP5<sup>+</sup> cells by qPCR (Fig. 3g-h). AQP5<sup>+</sup>  
162 cells routinely established organoids that were passaged for >3 months, whereas AQP5<sup>-</sup> cells  
163 never initiated organoids (Fig. 3i-j). The human pyloric organoids expressed AQP5  
164 heterogeneously, partially overlapping with KI67 (Extended Data Fig. 5k-l). Withdrawal of  
165 WNT3A, NOGGIN and FGF10 resulted in reduced *LGR5* and *AXIN2*, and elevated *MUC5AC*

166 and *TFF2* expression, indicating differentiation towards mucous lineages (Fig. 3k-l, Extended  
167 Data Fig. 5m-o).

168 RNASEQ was then performed on FACS-isolated AQP5+ pyloric cells from healthy human  
169 pylori, and the top hits validated by qPCR. We identified >500 differentially expressed genes  
170 that were significantly up/down-regulated by >4-fold in AQP5+ versus AQP5- populations (Fig.  
171 3m, top candidates in Supplementary Table 3). Q-PCR analysis validated 18 candidates as  
172 being enriched in the AQP5+ population (Extended Data Fig. 6a-e). Selected murine pyloric  
173 stem cell markers, including *AQP5*, *A4GNT* and *MUC6*, and an intestinal stem cell marker,  
174 *SMOC2*<sup>15</sup>, were upregulated in the AQP5+ fraction by RNASEQ and qPCR (Extended Data  
175 Fig. 6a). ISH confirmed *SMOC2* as being expressed in a subset of gland base cells (Extended  
176 Data Fig. 6f-f"). Gene Ontology analysis revealed that approximately half of the candidates  
177 were membrane expressed and had protein-binding activity (Fig. 3n, Extended Data Fig. 6b),  
178 suggesting that additional markers could be identified from our list to potentially further enrich  
179 for pyloric stem cells. Moreover, components of key signalling pathways (e.g. Wnt and Notch),  
180 chemokine signalling and extracellular matrix, and some uncharacterized genes, were also  
181 enriched in the AQP5+ population, highlighting the additional biological insight to be gained  
182 from the profile (Fig. 3n; Extended Data Fig. 6c-g).

183 Collectively, these data demonstrate AQP5's utility as a marker for isolating enriched  
184 populations of endogenous stem cells from human stomach epithelia for downstream  
185 purposes.

186

### 187 **Aqp5+ cells as source of gastric cancer**

188 We targeted conditional oncogenic mutations to pyloric stem cell-enriched populations using  
189 our new CreERT2 mouse models to evaluate their contribution to gastric cancer and  
190 circumvent the rapid lethality of Lgr5+ cell-driven cancer models<sup>2</sup>. To determine how often  
191 pathways are co-dysregulated in gastric cancer, we analysed transcriptomes of gastric cancer

192 patients from TCGA (n=155) and East Asian cohorts (n=42) for Wnt/ $\beta$ -catenin, PI3K and Ras  
193 signalling activities (Extended Data Fig. 7a-b), whose components are frequently mutated in  
194 gastric cancer<sup>3,16</sup>. Using published gene signatures<sup>17-19</sup>, we found that Wnt/ $\beta$ -catenin  
195 signalling was commonly hyper-activated in human gastric cancer (>80% in both patient  
196 cohorts), and frequently co-occurred with hyper-activation of PI3K and/or Ras signalling (57.1-  
197 64.3%)(Extended Data Fig. 7). We thus recapitulated these co-dysregulated pathways by  
198 crossing our pyloric CreERT2 drivers to conditional APC, PTEN and Kras<sup>G12D</sup> alleles and  
199 induced hyper-activation of the pathways at adulthood.

200

201 All mouse models developed sizeable tumours exclusively in the pylorus, with latencies  
202 ranging from 1-11 months post-induction (n=30/34, Extended Data Fig. 8a-g). In the tumours,  
203 which were classified as tubular-type gastric adenocarcinomas (WHO), malignant structures  
204 surrounded by stroma and inflammatory cells replaced normal glands. Sole hyper-activation  
205 of Kras<sup>G12D</sup> did not produce pyloric tumours (Extended Data Fig. 8h-i). Pylori of uninduced  
206 mice of the same cancer genotype lacking Cre were normal (Extended Data Fig. 8j).

207 Across all oncogene combinations, the tumor incidence in 2A-CreERT2 models was 100%  
208 compared to 82.6% in IRES-CreERT2 models (Fig. 4a), reflecting differences in Cre activation  
209 efficacies. The 2A-CreERT2 models displayed almost contiguous tumour growth, contrasting  
210 the multi-focal lesions in IRES-CreERT2 models (Extended Data Fig. 8b-g). Hyper-activation  
211 of Wnt/ $\beta$ -catenin signalling alone [APC<sup>fl/fl</sup> (A)] was sufficient to drive tumourigenesis, and co-  
212 activation of PI3K and/or Kras pathways [APC<sup>fl/fl</sup>;PTEN<sup>fl/fl</sup> (AP); APC<sup>fl/fl</sup>;PTEN<sup>fl/fl</sup>; Kras<sup>G12D</sup>  
213 (APK)] accelerated tumour development and progression (Extended Data Fig. 8a-g). We also  
214 observed focal invasions through the muscularis mucosae in A and AP models (IRES-  
215 CreERT2: 15.8%, 2A-CreERT2: 66.7%; Fig. 4a). As expected, intestinal tumors were never  
216 observed (Extended Data Fig. 8k-l).

217 We characterized all tumours to detail pathway activation, proliferation status, lineage marker  
218 expression and epithelia/stroma constitution. As there is no major phenotypic differences

219 between the different models, we present data from Aqp5-IRES-CreERT2;APK tumours, and  
220 focal invasions from Slc9a3-2A-CreERT2;AP tumours (Fig. 4b-c, i). The pyloric tumours and  
221 focal invasions were predominantly dTom+, confirming Aqp5+ or Slc9A3+ cells as their origins  
222 (Extended Data Fig. 9b, j). In contrast to the normal pylorus (Extended Data Fig. 9p-w), the  
223 gastric adenocarcinomas presented hyper-activation of Wnt/ $\beta$ -catenin, MAP kinase and  
224 phospho-AKT pathways, evidenced by elevated levels of nuclear/cytoplasmic  $\beta$ -catenin,  
225 MAPK and phospho-AKT expression respectively (Fig. 4f-h, m-o; Extended Data Fig. 9a).  
226 These regions were also highly proliferative, lacked Gif, Gast and Muc5ac expression  
227 (Extended Data Fig. 9d-g, l-o). In the Aqp5-IRES-CreERT2;APK model, dTom+ cells that  
228 retained E-cadherin expression were also found throughout the tumour stroma (Fig. 4e). In  
229 the Slc9a3-2A-CreERT2;AP model, E-cadherin+ cells infiltrated through the muscularis  
230 mucosae (Fig. 4l). Immunostaining for Aqp5-GFP reporter expression revealed Aqp5  
231 expression in a subpopulation of the pyloric tumours, some of which were Ki67+ (Fig. 4d, k,  
232 p). Many of the Aqp5+ cells in the tumours co-expressed *Lgr5*, with elevated Aqp5 expression  
233 in tumours compared to adjacent normal mucosa (Extended Data Fig. 9h-h"). There was a  
234 low incidence of tumours within non-gastrointestinal organs, such as the salivary gland (<25%  
235 in Aqp5-IRES-CreERT2-driven cancer models), which did not impact survival to preclude  
236 gastric adenocarcinoma development (Extended Data Fig. 9i-i'). Thus, our mouse models  
237 support pyloric stem cell-enriched populations as being a source of invasive, Wnt-driven  
238 gastric cancer and are valuable for modelling gastric cancer *in vivo*.

239

#### 240 **Aqp5+ tumour cells display *ex vivo* stemness**

241 We then determined if Aqp5+ tumour cells behave differently from their Aqp5- counterparts.  
242 After confirming that the Aqp5-GFP reporter recapitulated endogenous Aqp5 expression in  
243 the tumours (Extended Data Fig. 9x-x'), we cultured sorted Aqp5-GFP+ and GFP- cells  
244 (Extended Data Fig. 9y-z"). Aqp5-GFP+ tumour cells reproducibly generated organoids that  
245 could be serially propagated in the absence of exogenous growth factors, while Aqp5-GFP-

246 tumour populations never produced organoids, despite containing Ki67+ cells (Fig. 4p-s).  
247 Moreover, though Aqp5-GFP+ normal cells could initiate organoids with growth factors, they  
248 died upon growth factor removal (Fig. 4r-s). These data suggest that the stem potential of the  
249 tumour is found within the Aqp5+ compartment.

250

## 251 **AQP5 expression in human gastric cancer**

252 We surveyed AQP5 expression in human gastric cancer by immunostaining on a tissue  
253 microarray of 145 distal gastric cancer samples comprising intestinal, diffuse and mixed  
254 subtypes with variable grades of differentiation. AQP5 was expressed in most intestinal,  
255 diffuse and mixed cases (Extended Data Fig. 10a-e). Contrasting normal pylorus, 96.1% of  
256 the tumour samples displayed cytoplasmic AQP5 expression, 37.9%, 3.9% and 37.9% had  
257 membranous, nuclear and multiple localizations of AQP5 respectively (Extended Data Fig.  
258 10a-e). While intracellular AQP5 localization has been reported in other cancers<sup>20-22</sup>, its  
259 functional significance is unknown.

260 In full sections of 54 advanced human distal gastric adenocarcinomas and 12 metastatic  
261 lesions, most expressed AQP5 (Extended Data Fig. 10f). Cytoplasmic AQP5 was observed in  
262 all AQP5+ samples, while membranous/luminal, nuclear and multiple sites of AQP5  
263 localization were found in 53.7%, 9.8% and 53.7% of the samples respectively (Extended Data  
264 Fig. 10f-j). In 67.7% of the sections, submucosal malignant cells expressed more AQP5 than  
265 their mucosal counterparts (Extended Data Fig. 10g-j, o, p). AQP5 was expressed in poorly  
266 cohesive tumour cells in 70% of the cohort (Extended Data Fig. 10j, o). All AQP5+ cells in the  
267 submucosa retained E-Cadherin expression, and a subset co-expressed KI67 (Extended Data  
268 Fig. 10k-n). 46.2% of intestinal metaplasia cases, which is strongly correlated with gastric  
269 cancer<sup>23,24</sup>, displayed mild to moderate AQP5 expression (Extended Data Fig. 10o, q). AQP5  
270 was also weakly expressed in a subset of signet ring cells in 66.7% of the samples (Extended

271 Data Fig. 10o, r). 83.3% of the metastatic lesions with AQP5+ primary tumours harboured  
272 AQP5+ tumour cells in the lymph node (Extended Data Fig. 10o, s).

273 Our broad survey shows that AQP5 is commonly expressed in primary and metastases of  
274 intestinal and diffuse subtypes of gastric cancer.

275

276 Efforts to exploit the therapeutic potential of stem cells require functionally validated markers  
277 for their prospective isolation. For the first time, we purify enriched populations of human  
278 pyloric stem cells and demonstrate the direct contribution of murine Aqp5+ cells to gastric  
279 carcinogenesis. Though the expression of secretory markers like Gif and Muc6 may not  
280 conform to the classical “undifferentiated” stem cell dogma, it is well established in liver and  
281 lung that more specialized cells can serve as homeostatic stem cells<sup>25–28</sup>, an emerging trend  
282 in epithelial organs<sup>29</sup>. While Aqp5 is known for regulating water transport in healthy tissues<sup>6</sup>,  
283 it is increasingly implicated in cancers as a driver of proliferation and invasiveness *in vitro*<sup>30–</sup>  
284 <sup>34</sup>. Various human cancers, including gastric, breast, soft tissue sarcoma, lung, oesophageal  
285 and colorectal cancers, present high AQP5 expression<sup>21,22,33,35–37</sup>. We show that AQP5 is  
286 expressed in most human primary tumours and metastases of intestinal and diffuse gastric  
287 cancer subtypes. Interestingly, we found that tumour-resident Aqp5+ cells in our gastric cancer  
288 mouse model selectively exhibited *ex vivo* stem potential, indicating that the Aqp5+ tumour  
289 population harbours cancer stem cells. Future evaluation of the stem potential of AQP5+ in  
290 human gastric cancers using our new antibody-based isolation protocols will potentially reveal  
291 novel opportunities for developing more effective cancer therapeutics.

292

293 **References**

- 294 1. Barker, N. *et al.* Lgr5+ve Stem Cells Drive Self-Renewal in the Stomach and Build  
295 Long-Lived Gastric Units In Vitro. *Cell Stem Cell* **6**, 25–36 (2010).
- 296 2. Barker, N. *et al.* Crypt stem cells as the cells-of-origin of intestinal cancer. *Nature*  
297 (2009). doi:10.1038/nature07602
- 298 3. Network, T. C. G. A. R. *et al.* Comprehensive molecular characterization of gastric  
299 adenocarcinoma. *Nature* **513**, 202 (2014).
- 300 4. Barker, N. *et al.* Identification of stem cells in small intestine and colon by marker  
301 gene Lgr5. *Nature* **449**, 1003–1007 (2007).
- 302 5. Tian, H. *et al.* A reserve stem cell population in small intestine renders Lgr5-positive  
303 cells dispensable. *Nature* **478**, 255–9 (2011).
- 304 6. Direito, I., Madeira, A., Brito, M. A. & Soveral, G. Aquaporin-5: from structure to  
305 function and dysfunction in cancer. *Cell. Mol. Life Sci.* **73**, 1623–1640 (2016).
- 306 7. Grun, D. *et al.* Single-cell messenger RNA sequencing reveals rare intestinal cell  
307 types. *Nature* **525**, 251–255 (2015).
- 308 8. Choi, E. *et al.* Lrig1+ gastric isthmal progenitor cells restore normal gastric lineage  
309 cells during damage recovery in adult mouse stomach. *Gut* gutjnl-2017-313874  
310 (2017). doi:10.1136/gutjnl-2017-313874
- 311 9. Matsuo, J. *et al.* Identification of Stem Cells in the Epithelium of the Stomach Corpus  
312 and Antrum of Mice. *Gastroenterology* **152**, 218-231.e14 (2017).
- 313 10. Sigal, M. *et al.* Stromal R-spondin orchestrates gastric epithelial stem cells and gland  
314 homeostasis. *Nature* **548**, 451–455 (2017).
- 315 11. Hayakawa, Y. *et al.* CCK2R identifies and regulates gastric antral stem cell states and  
316 carcinogenesis. *Gut* **64**, 544–553 (2015).
- 317 12. Arnold, K. *et al.* Sox2 + adult stem and progenitor cells are important for tissue  
318 regeneration and survival of mice. *Cell Stem Cell* (2011).  
319 doi:10.1016/j.stem.2011.09.001
- 320 13. Funaki, H. *et al.* Localization and expression of AQP5 in cornea, serous salivary  
321 glands, and pulmonary epithelial cells. *Am. J. Physiol.* (1998).

- 322 14. Matsuzaki, T. *et al.* Expression and immunolocalization of water-channel aquaporins  
323 in the rat and mouse mammary gland. *Histochem. Cell Biol.* (2005).  
324 doi:10.1007/s00418-005-0753-x
- 325 15. Muñoz, J. *et al.* The Lgr5 intestinal stem cell signature: Robust expression of  
326 proposed quiescent ' +4' cell markers. *EMBO J.* (2012). doi:10.1038/emboj.2012.166
- 327 16. Muratani, M. *et al.* Nanoscale chromatin profiling of gastric adenocarcinoma reveals  
328 cancer-associated cryptic promoters and somatically acquired regulatory elements.  
329 *Nat. Commun.* (2014). doi:10.1038/ncomms5361
- 330 17. Zhang, Y. *et al.* A Pan-Cancer Proteogenomic Atlas of PI3K/AKT/mTOR Pathway  
331 Alterations. *Cancer Cell* (2017). doi:10.1016/j.ccell.2017.04.013
- 332 18. Pek, M. *et al.* Oncogenic KRAS-associated gene signature defines co-targeting of  
333 CDK4/6 and MEK as a viable therapeutic strategy in colorectal cancer. *Oncogene*  
334 (2017). doi:10.1038/onc.2017.120
- 335 19. Van der Flier, L. G. *et al.* The Intestinal Wnt/TCF Signature. *Gastroenterology* (2007).  
336 doi:10.1053/j.gastro.2006.08.039
- 337 20. Lambertz, N. *et al.* Expression of aquaporin 5 and the AQP5 polymorphism A(-1364)C  
338 in association with peritumoral brain edema in meningioma patients. *J. Neurooncol.*  
339 (2013). doi:10.1007/s11060-013-1064-z
- 340 21. Shimizu, H. *et al.* The expression and role of Aquaporin 5 in esophageal squamous  
341 cell carcinoma. *J. Gastroenterol.* (2014). doi:10.1007/s00535-013-0827-9
- 342 22. Zhu, Z. *et al.* Expression of AQP3 and AQP5 as a prognostic marker in triple-negative  
343 breast cancer. *Oncol. Lett.* **16**, 2661–2667 (2018).
- 344 23. Kinoshita, H., Hayakawa, Y. & Koike, K. Metaplasia in the stomach—precursor of  
345 gastric Cancer? *International Journal of Molecular Sciences* (2017).  
346 doi:10.3390/ijms18102063
- 347 24. Jencks, D. S. *et al.* Overview of current concepts in gastric intestinal metaplasia and  
348 gastric cancer. *Gastroenterol. Hepatol.* (2018).
- 349 25. Rawlins, E. L., Clark, C. P., Xue, Y. & Hogan, B. L. M. The Id2+ distal tip lung  
350 epithelium contains individual multipotent embryonic progenitor cells. *Development*  
351 (2009). doi:10.1242/dev.037317

- 352 26. Barkauskas, C. E. *et al.* Type 2 alveolar cells are stem cells in adult lung. *J. Clin.*  
353 *Invest.* (2013). doi:10.1172/JCI68782
- 354 27. Desai, T. J., Brownfield, D. G. & Krasnow, M. A. Alveolar progenitor and stem cells in  
355 lung development, renewal and cancer. *Nature* (2014). doi:10.1038/nature12930
- 356 28. Wang, B., Zhao, L., Fish, M., Logan, C. Y. & Nusse, R. Self-renewing diploid Axin2(+)  
357 cells fuel homeostatic renewal of the liver. *Nature* **524**, 180–5 (2015).
- 358 29. Post, Y. & Clevers, H. Defining Adult Stem Cell Function at Its Simplest: The Ability to  
359 Replace Lost Cells through Mitosis. *Cell Stem Cell* **25**, 174–183 (2019).
- 360 30. Kang, S. K. *et al.* Aquaporin 5 (AQP5) is a novel signaling molecule triggering  
361 Ras/ERK/retinoblastoma (Rb) signaling pathway in colon cancer cell lines. *Mol.*  
362 *Cancer Ther.* **6**, B115 LP-B115 (2007).
- 363 31. Woo, J. *et al.* The effect of aquaporin 5 overexpression on the Ras signaling pathway.  
364 *Biochem. Biophys. Res. Commun.* (2008). doi:10.1016/j.bbrc.2007.12.073
- 365 32. Woo, J. *et al.* Overexpression of AQP5, a putative oncogene, promotes cell growth  
366 and transformation. *Cancer Lett.* (2008). doi:10.1016/j.canlet.2008.01.029
- 367 33. Chae, Y. K. *et al.* Expression of aquaporin 5 (AQP5) promotes tumor invasion in  
368 human non small cell lung cancer. *PLoS One* (2008).  
369 doi:10.1371/journal.pone.0002162
- 370 34. Huang, Y.-H. *et al.* Aquaporin 5 promotes the proliferation and migration of human  
371 gastric carcinoma cells. *Tumour Biol.* (2013). doi:10.1007/s13277-013-0712-4
- 372 35. Shimasaki, M., Kanazawa, Y., Sato, K., Tsuchiya, H. & Ueda, Y. Aquaporin-1 and -5  
373 are involved in the invasion and proliferation of soft tissue sarcomas. *Pathol. - Res.*  
374 *Pract.* **214**, 80–88 (2018).
- 375 36. Wang, W. *et al.* Expression of AQP5 and AQP8 in human colorectal carcinoma and  
376 their clinical significance. *World J. Surg. Oncol.* (2012). doi:10.1186/1477-7819-10-  
377 242
- 378 37. Shen, L. *et al.* Expression profile of multiple aquaporins in human gastric carcinoma  
379 and its clinical significance. *Biomed. Pharmacother.* (2010).  
380 doi:10.1016/j.biopha.2009.12.003

381

382 **Figure legends**

383

384 Fig. 1: Comparative profiling of Lgr5 populations in gastrointestinal tissues yields new pyloric  
385 specific markers

386 (a) Heatmap of transcriptomes of Lgr5-EGFP<sup>Hi</sup>, Lgr5-EGFP<sup>Lo</sup> and unsorted populations from  
387 mouse pylorus, small intestine and colon (n=4, 2, 3, biological replicates respectively) from  
388 Lgr5-EGFP-IRES-CreERT2 mice. Candidates are enriched only in pylorus-GFP<sup>Hi</sup> population  
389 (black box).

390 (b) Overlap of candidate markers from Lgr5-EGFP-IRES-CreERT2 (above) and Lgr5-DTR-  
391 EGFP (n=4 biological replicates) models (statistical significance assessed by hypergeometric  
392 distribution).

393 (c) Shortlisted pylorus-specific markers.

394 (d) Relative *Aqp5* expression (qPCR) in gastrointestinal populations (n=2 technical replicates  
395 of pooled sample from 8 mice, means represented).

396 (e-j) *In situ* hybridization (ISH) expression of candidate markers in pylorus (n=3 mice).

397 (k-m) *Aqp5* expression with *Lgr5* in pylorus by immunostaining (k,m) and ISH (l) (n=3 mice).

398 Scale bars represent 25  $\mu$ m.

399

400 Fig. 2: Pyloric Aqp5+ population contains stem cells *in vivo*

401 (a) Aqp5-EGFP-IRES-CreERT2 transgene.

402 (b-e) EGFP co-immunostaining in Aqp5-EGFP-IRES-CreERT2 pylorus with Gif (b), Gastrin  
403 (c), Mucin5ac (d) and Chromogranin A (ChgA, e) (n=3 mice).

404 (f-i) Lineage tracing of Aqp5-EGFP-IRES-CreERT2;tdTomato<sup>LSL</sup> pylori at 20 hours (f), 5 days  
405 (g), 1 month (h) and 6 months (i) (n=3 mice).

406 (j-m) Co-immunostaining of tdTomato with ChgA (j), Gastrin (k), GIF (l) and Mucin5ac (m) (n=3  
407 mice per marker).

408 (n) FACS gating for sorting Aqp5+ and Aqp5- cells (means $\pm$ s.e.m.; n=6 biological replicates).

409 (o-p) Relative *Aqp5* (o) and *Lgr5* (p) expression (qPCR) in sorted populations (means± s.e.m.;  
410 n=10 biological replicates).

411 (q) *Lgr5* and candidate marker enrichment in volcano plot of differentially expressed genes in  
412 *Aqp5*<sup>+</sup> population by microarray (n=4 biological replicates, p-value from one-way ANOVA in  
413 Partek Analysis Software).

414 (r-s) Outgrowth efficiency of single antibody-mediated FACS-sorted *Aqp5*<sup>+</sup> and *Aqp5*<sup>-</sup> cells (r)  
415 with representative images (s) (n=5 biological replicates).

416 (t) Longevity and highest passage number of organoids from *Aqp5*<sup>+</sup> and *Aqp5*<sup>-</sup> cells (n=3  
417 biological replicates).

418 (u) Organoid differentiation protocol.

419 (v-x) Relative *Aqp5* (v), *Lgr5* (w) and *Muc5ac* (x) expression (qPCR) in *Aqp5*<sup>+</sup> cell-derived  
420 organoids on day 4 of differentiation (n=5 biological replicates).

421 Scale bars represent 25 µm in (b-m), and 100 µm in (s). Graphs represent means±s.e.m. with  
422 two-sided t-test (r), (t), (v-x).

423

424 Fig. 3: Human pyloric AQP5<sup>+</sup> cells are stem cells *ex vivo*

425 (a) Immunostaining of AQP5 in normal human pylorus (n=3 biological replicates).

426 (b-d) AQP5 and LGR5 expression in pylorus (b) near gland surface (c) and base (d) by ISH  
427 (n=3 biological replicates).

428 (e-f) AQP5 and KI67 co-localization (arrowheads, n=3 biological replicates).

429 (g) FACS gating for sorting human AQP5<sup>+</sup> and AQP5<sup>-</sup> cells (means±SEM; n=4 biological  
430 replicates).

431 (h) Relative AQP5 expression (qPCR) in FACS-sorted AQP5<sup>+</sup> and AQP5<sup>-</sup> cells (n=3 biological  
432 replicates).

433 (i-j) Outgrowth efficiency of single AQP5<sup>+</sup> and AQP5<sup>-</sup> cells *in vitro* (i) with representative image  
434 (j) (n=3 biological replicates).

435 (k-l) Relative LGR5 (k) and MUC5AC (l) expression in (qPCR) AQP5<sup>+</sup> cell-derived organoids  
436 on day 4 of differentiation (n=3 biological replicates).

437 (m) Heatmap of 200 genes with highest variation between normal human pylorus AQP5+ and  
438 AQP5- populations by RNASEQ (n=8 biological replicates).

439 (n) GO terms associated with genes significantly enriched in AQP5+ population.

440 Scale bars represent 100µm in (a),(b),(e),(j) and 50µm in (c),(d),(f). Graphs are presented as  
441 means± s.e.m.; two-sided t-test.

442

443 Fig. 4: Aqp5+ population is a source of Wnt-driven, invasive gastric cancer

444 (a) Characteristics of gastric cancer models.

445 (b-h) Characterization of Aqp5-EGFP-IRES-CreERT2;APK intramucosal gastric  
446 adenocarcinoma. H&E stain of entire pyloric region (b) and tumour (green box) (c).

447 Immunostaining of the tumour region in (b) for Aqp5-GFP (d), E-cadherin (e), phospho-AKT  
448 (f), MAPK (g) and β-catenin (h) in the tumour region (b). (h) is a higher magnification of

449 Extended Data Fig. 12a.

450 (i-o) Characterization of Slc9a3-2A-CreERT2;AP gastric adenocarcinoma. H&E of entire  
451 pyloric region (i) and the focal invasion (j). Immunostaining for Aqp5 (k), E-cadherin (l),

452 phospho-AKT (m), MAPK (n) and β-catenin (o) in the focal invasion.

453 (p) Co-staining of Aqp5-GFP, Ki67 and E-cadherin in Aqp5-CreERT2;APK pyloric tumour.

454 (s-u) Organoid assay with Aqp5-GFP+ GFP- tumour cells (n=3 biological replicates). (q)

455 Initiation frequencies of Aqp5-GFP+ tumour cells (APK-GFP+) versus Aqp5-GFP- tumour cells  
456 (APK-GFP-). Paired two-sided t-test, means±s.e.m. (r) Means and individual longevities of

457 organoids derived from APK-GFP+, APK-GFP- and Norm-GFP+ (Aqp5-GFP+ cells from  
458 normal pylorus) cells seeded with exogenous growth factors (GF) for a week and without GF

459 for the next 4 weeks. (s) Representative images of organoids derived from APK-GFP+ cells  
460 and Norm-GFP+ cells in the respective GF conditions.

461 Scale bars represent 1 mm in (b),(i), 100 µm in (d-h), (j-o), 20 µm in (p), and 500 µm in (s).

462

## 463 **Methods**

### 464 **Mice**

465 For exon 1-knockins, an EGFP-IRES-CreERT2 cassette was inserted immediately  
466 downstream of the start codons of *Aqp5*, *A4gnt*, *Spp1* and *Slc9a3* gene loci by homologous  
467 recombination in embryonic stem cells as illustrated in Extended Data Fig. 3a. For 3' UTR-  
468 knockins, a 2A-CreERT2, 2A-EGFP or 2A-DTR cassette was inserted immediately before the  
469 stop codon of *Aqp5*, *Lgr5* and/or *Slc9a3* gene loci by homologous recombination in embryonic  
470 stem cells as illustrated in Extended Data Fig. 3b, thereby preserving the intact protein-coding  
471 region and endogenous expression of the genes. Rosa26-tdTomato<sup>LSL</sup> (Ai14) (JAX ID 007914)  
472 mice<sup>38</sup> were obtained from Jackson Labs. *Lgr5*-EGFP-IRES-CreERT2<sup>4</sup> (JAX ID 008875),  
473 *Lgr5*-DTR-EGFP (MGI ID 5294798)<sup>5</sup>, *Kras*<sup>LSL-G12D</sup> (JAX ID 019104)<sup>39</sup>, APC<sup>fl/fl</sup> (MGI ID  
474 1857966)<sup>40</sup> and PTEN<sup>fl/fl</sup> (MGI ID 2182005)<sup>41</sup> mice have been described previously. All Cre and  
475 EGFP lines are bred as heterozygotes except *A4gnt*-IRES-CreERT2 and *Spp1*-IRES-  
476 CreERT2 mice, which are bred as homozygotes. All animal experiments were approved by  
477 the "Institutional Animal Care and Use Committee" of Singapore and performed in compliance  
478 with all relevant ethical regulations. Maximum tumour size allowed by IACUC is 20mm in any  
479 dimension and none of the experiments exceeded this limit. For all experiments, adult animals  
480 (not selected for gender) with a minimum age of 7-8 weeks were used. The experiments were  
481 not randomized, and there was no blinded allocation during experiments and outcome  
482 assessment. No statistical method was used to pre-determine sample size. Genotyping  
483 primers are collated in Supplementary Table 4. Mouse lines are available upon request.

### 484 **Human material**

485 Normal human pylorus for FACS was provided by K.G. Yeoh, J. So and A. Shabbir, NUS  
486 Department of Medicine and Pathology (granted under protocol 11-167E) and N. Inaki and T.  
487 Tsuji, Ishikawa Prefectural Central Hospital. Informed consent was obtained from all patients  
488 and experiments were performed in compliance with all relevant ethical regulations. Human  
489 distal cancer FFPE sections were provided by NUS Department of Medicine and Pathology

490 (granted under protocol-11-167E) and Leeds Teaching Hospitals NHS Trust, Leeds, UK  
491 (granted under protocol CA01\_122).

## 492 **Animal treatment**

493 Mice were each injected with tamoxifen dissolved in sunflower oil intraperitoneally at 4 mg  
494 tamoxifen/30g body weight. Diphtheria Toxin (DT)-treated mice were injected with a single  
495 dose of DT dissolved in PBS intraperitoneally at 0.5 ug DT/30g body weight.

## 496 **Gland isolation, cell dissociation and flow cytometry**

### 497 *Murine pylorus*

498 Murine pylorus was incubated in chelation buffer (5.6 mM sodium phosphate, 8 mM potassium  
499 phosphate, 96.2 mM sodium chloride, 1.6 mM potassium chloride, 43.4 mM sucrose, 54.9 mM  
500 D-sorbitol, 1 mM dithiothreitol) with 5 mM EDTA at 4°C for 2 hours. Glands were isolated by  
501 repeated pipetting of finely chopped pylorus tissue in cold chelation buffer. Chelation buffer  
502 containing isolated glands was filtered through 100 µm filter mesh, and centrifuged at 720g at  
503 4°C for 3 min. The pellet was resuspended in TrypLE (Life Technologies) with DNaseI  
504 (0.8U/µL) (Sigma) and incubated at 37°C for 10 min with intermittent trituration for digestion  
505 into single cells. Digestion was quenched by dilution with cold HBSS buffer. The suspension  
506 was centrifuged at 720g at 4°C for 3 min. For anti-Aqp5 antibody stain, the pellet was  
507 resuspended in HBSS with 2% fetal bovine serum (FBS, Hyclone) with anti-Aqp5-AF647  
508 (Abcam, ab215225) at 1:500 dilution and incubated on ice at 30min in the dark. The pellet was  
509 subsequently washed twice with cold HBSS and spun at 800g for 3min at 4°C. The pellet was  
510 resuspended in HBSS with 2% FBS. Before sorting, 1 µg/ml propidium iodide (Life  
511 Technologies) was added to the cell suspensions, filtered through a 40µm strainer, and sorted  
512 on BD Influx Cell Sorter (BD Biosciences). Cells were collected in RLT Plus buffer (Qiagen)  
513 for RNA extraction or HBSS with 2% FBS and 1% PenStrep (Gibco) for organoid culture.

514

515

516 *Human pylorus*

517 Human pylorus was collected in Advanced DMEM/F-12 media with 10 mM HEPES, 2 mM  
518 Glutamax (incubation buffer, all from Life Technologies), supplemented with 1X Anti-Anti (Life  
519 Technologies) and 1mM N-acetylcysteine (Sigma). After at least three washes in HBSS, the  
520 pylorus was finely chopped and digested in incubation buffer supplemented with 1mg/mL  
521 Collagenase (Gibco) and 2mg/mL Bovine Serum Albumin (Sigma) for 30 min at 37°C with  
522 intermittent mixing. The remainder of the processing protocol is identical to that for the murine  
523 tissue described earlier. Cells for organoid culture were collected in organoid culture medium  
524 with growth factors and 0.2% Growth factor-reduced Matrigel (Corning) (v/v).

525 **Organoid culture**

526 Organoid culture of FACS-isolated single human and murine pylorus cells were performed as  
527 described previously<sup>42</sup>. Briefly, single cells were resuspended in growth factor-reduced  
528 Matrigel (Corning) and cultured in basal media [Advanced DMEM/F-12 media with 10mM  
529 HEPES, 2mM Glutamax, 1X N2, 1X B27 (all Invitrogen), N-acetyl-cysteine (Sigma), Primocin  
530 (Invivogen)] supplemented with these growth factors - EGF (Invitrogen), Gastrin (Sigma),  
531 FGF10 (Peprotech), Noggin (Peprotech), Wnt3a (Millipore), R-spondin and ROCK inhibitor  
532 Y27632 (Sigma). A83-01 (Tocris) is also added to human pyloric cultures. Mouse cancer  
533 organoids were grown in only basal media after first week of culture. Organoids were  
534 passaged when confluent, at least once a week. Only organoids beyond 100 µm and 200 µm  
535 in diameter with a clear central lumen are scored as organoids for Fig. 4 and Fig. 5  
536 respectively.

537 **RNA isolation and qPCR**

538 Tissues were lysed in Trizol (Qiagen) and single cells were lysed in RLT Plus buffer (Qiagen).  
539 RNA was subsequently isolated with RNeasy Universal Plus kit (Qiagen) and cDNA was

540 generated with Superscript III (Life Technologies) according to manufacturer's instructions.  
541 qPCR was performed with a minimum of three biological replicates per gene using SYBR  
542 Green dye (Promega) according to the manufacturer's instructions and ran on StepOne or  
543 Quantstudio7 qPCR machines (Applied Biosystems). Analysis was carried out using double  
544 CT method on Step One Software on the respective qPCR machines (Applied Biosystems).  
545 qPCR validation of top candidates from RNASEQ was performed on 2-4 ng of SPIA-amplified  
546 cDNA derived from the Ovation Pico WTA system (Nugen Technologies) due to limitation of  
547 RNA availability. In the event any of the samples for a specific target does not amplify, the  
548 relative expression values of all the samples for that target are increased by one to allow  
549 visualization of the values on a log scale. Sequences of qPCR primers are collated in  
550 Supplementary Table 4.

## 551 **Transcriptome profiling and analysis**

### 552 *Single cell RNAseq CEL-Seq and RaceID*

553 Single Lgr5-EGFP<sup>Hi</sup> pyloric epithelial cells from Lgr5-DTR-EGFP mice<sup>5</sup> were isolated by FACS  
554 (as described earlier) and collected in each well of 96-well plates. Total RNA extracted from  
555 each cell was used to generate single-cell RNA expression libraries as described<sup>48</sup>. A total of  
556 285 Lgr5-EGFP<sup>Hi</sup> cells from three mice were sequenced on Illumina HighSeq 2500 instrument  
557 using 101 base-pair paired end sequencing. K-means clustering in RaceID was used to  
558 delineate clusters of subpopulations as previously described<sup>20</sup>.

### 559 *Microarray and analysis*

560 Labelling, hybridization and washing protocols for microarrays were performed according to  
561 Origene instructions. RNA quality was first determined by assessing the integrity of the 28s  
562 and 18s ribosomal RNA bands on Agilent RNA 60000 Pico LabChips in an Agilent 2100  
563 Bioanalyser (Agilent Technologies). A minimum of 2ng of RNA was used to generate SPIA-  
564 amplified cDNA using the Ovation Pico WTA system (Nugen Technologies). Five micrograms  
565 of SPIA-amplified purified cDNA was then fragmented and biotin-labelled using the Nugen

566 Encore Biotin module (Nugen Technologies). Microarray was performed using the Affymetrix  
567 Mouse ST v2.0 GeneChips (Affymetrix), which consists of more than 28,000 probes for  
568 previously annotated genes. The individual microarrays were washed and stained in an  
569 Affymetrix Fluidics Station 450, and hybridized probe fluorescence was detected using the  
570 Affymetrix G3000 GeneArray Scanner. Image analysis was carried out on the Affymetrix  
571 GeneChip Command Console v2.0 using the MAS5 algorithm. CEL files were generated for  
572 each array and used for gene expression analysis. The CEL files were then processed in R  
573 (v3.2.3) with the Bioconductor (v3.2) libraries 'oligo' (v1.34.2), 'pd.mogene.2.0.st' (v3.14.1)  
574 and 'limma' (v3.26.8). We used Robust Multi-array Average (RMA) to perform background  
575 correction and normalization with the 'rma' function implemented in the 'oligo' package ('target'  
576 parameter was set to 'core' to obtain expression values at the gene level). The experimental  
577 design was stored as a single factor with individual levels for each combination of Lgr5-GFP  
578 level (high, low, negative) or Aqp5 status (positive, negative). Linear models were fitted to the  
579 expression data with the function 'lmFit' (default parameters). The relevant contrasts were  
580 fitted with 'contrasts.fit' (default parameters); differential expression was tested with 'eBayes'  
581 (default parameters). Differential gene expression was analyzed using Partek Genomics Suite  
582 software (Partek). Relative gene expressions are depicted as single values as given by Partek  
583 Analysis Software. Gene Set Enrichment Analysis was performed using the GSEA v6.1<sup>46,47</sup>.

#### 584 *RNASEQ*

585 AQP5+ and AQP5- cells were collected directly into RLT Plus buffer by FACS sorting. Total  
586 RNA was isolated using Qiagen RNeasy Micro Kit (QIAGEN). RNA quality was first  
587 determined by assessing the integrity of the 28s and 18s ribosomal RNA bands on Agilent  
588 RNA 60000 Pico LabChips in an Agilent 2100 Bioanalyser (Agilent Technologies). Amplified  
589 cDNA library was prepared according to manufacturer's instructions with SMARTer Stranded  
590 Total RNA-Seq Kit v2 - Pico Input Mammalian (Takara) using 10ng of input Total RNA.  
591 Indexed 150bp paired end sequencing was performed on HiSeq 2500 (Illumina) and Illumina  
592 Real-Time Analysis (RTA) software was used for base-calling to generate Fastq files. The

593 reads were mapped to Genome Reference Consortium Human Build 38 patch release 12  
594 (GRCh38.p12) with STAR software version 2.5.3a with the following options issued: --  
595 outFilterType BySJout, --outFilterMultimapNmax 10, --alignSJoverhangMin 15, --  
596 alignSJDBoverhangMin 1, --outFilterMismatchNmax 12, --outFilterMatchNminOverLread 0.4,  
597 --alignIntronMin 20, --alignIntronMax 2000000, --outSAMattrIHstart 0, --outSAMmapqUnique  
598 244, --outMultimapperOrder Random, --outReadsUnmapped None, --outFilterIntronMotifs  
599 None, --outSAMmode Full, --outSAMattributes All --quantMode GeneCounts, --  
600 clip3pAdapterSeq  
601 AATGATACGGCGACCACCGAGATCTACACTCTTTCCCTACACGACGCTCTTCCGATCT.  
602 Counts per sample were subsequently concatenated in a statistical software, R version 3.2.3,  
603 and reads were normalized with Trimmed mean of M values (TMM) normalisation as  
604 implemented in edgeR version 3.12.1 (with limma\_3.26.9). Differential expression testing was  
605 performed with the edgeR function “glmQLFit” using a design matrix that took sample batches  
606 and AQP5 status into account. Differentially expressed genes (DEGs) were those with more  
607 than 2-fold change between AQP5+ and AQP5- samples, with FDR<0.05. Due to likely  
608 inclusion of immune cells in the profile, immune-related genes<sup>43</sup> were omitted, resulting in a  
609 final list of >500 DEGs. Gene Ontology, Overrepresentation Analysis (ORA) and PANTHER  
610 Pathway analysis of the DEGs were performed on the PANTHER Classification System<sup>44</sup>  
611 using default parameters.

### 612 *Transcriptomic pathway signature analysis of human gastric cancer*

613 Level 3 TCGA RNA-seq normalized matrix for 415 GC and 35 normal gastric samples and  
614 their corresponding clinical information were downloaded from the Broad Institute TCGA  
615 Genome Data Analysis Center (GDAC) Firehose (<https://gdac.broadinstitute.org/>). Gene  
616 expression data of 200 GC and 100 matched normal gastric samples were generated using  
617 Affymetrix Human Genome U133 Plus 2.0 Array (GSE15459) and processed as described  
618 previously<sup>16</sup>. All normal samples and only tumours of antral or pyloric origin were included for  
619 analysis. To determine activity of PI3K, Wnt and KRAS pathways in primary tumours, we

620 utilized published pathway signatures by several groups: KRAS signature based on differential  
621 gene expression analysis between high KRAS mutation and low KRAS mutation/wildtype CRC  
622 tumours<sup>18</sup>; PI3K signature composed of genes modulated *in vitro* by PI3K inhibitors, according  
623 to the CMap signature<sup>17</sup> and lastly, intestinal Wnt signature defined by profiling CRC cell lines  
624 carrying an inducible block of the Wnt pathway and differential gene expression analysis of  
625 human colon adenoma and adenocarcinomas versus normal colonic epithelium<sup>19</sup>. For each  
626 pathway signature, only up-regulated genes in pathway activation were selected for  
627 downstream analysis.

628 To quantify the relative activation level in a specific oncogenic pathway, we derived a “ $\mu$  score”  
629 for each sample profile. In brief, the transcriptomic “ $\mu$  score” was defined as the average of  
630 standardized expression values of those up-regulated genes in a specific oncogenic pathway  
631 (after the log-transformed values centred to the standard deviation from the median across  
632 the samples included in the analysis). For each oncogenic pathway, “ $\mu$  scores” were  
633 calculated for all normal samples, and the “ $\mu$  score” at the 90% percentile of the normal  
634 samples was used as the cut-off to define a pathway as “hyperactivated”. The “ $\mu$  score” for  
635 each tumour was determined and a “ $\mu$  score” higher than the cut-off was considered to be  
636 “hyperactivated” for that particular pathway. For each combination of pathways (Wnt,  
637 Wnt/PI3K or Wnt/PI3K/Kras), the concurrence rate was given by the frequency of tumours that  
638 were “hyperactivated” in all the pathways in question.

## 639 **Histology**

640 *Immunohistochemistry (IHC) and immunofluorescence (IF).*

641 IHC and IF were performed according to standard protocols. In summary, tissues were fixed  
642 in 4% paraformaldehyde/PBS (w/v) overnight at 4°C, and processed into paraffin blocks. 8  $\mu$ m  
643 sections from the paraffin blocks and tissue microarray slides were deparaffinated and  
644 rehydrated, followed by antigen retrieval via heating to 121°C in a pressure cooker in standard  
645 10mM citric acid pH6 buffer, a commercial citrate pH 6.1 buffer (S1699, DAKO) or Tris/EDTA

646 buffer, pH 9.0 (S2367, DAKO). Primary antibodies used were chicken anti-EGFP (1:2,000,  
647 Abcam, ab290), rabbit anti-EGFP (1:200; Cell Signalling, 2956S), rabbit anti-Ki67 (1:200;  
648 Thermofisher, MA5-14520), rabbit anti-GIF (1:10,000; provided by D. H. Alpers, Washington  
649 University School of Medicine, USA), rabbit anti-RFP (1:200; Rockland, 600-401-379), rabbit  
650 anti-aquaporin5 (1:200, Santa Cruz, SC-28628 and 1:500, LSBio, LS-C756566), rabbit anti-  
651 Slc9a3 (1:200; Santa Cruz, SC-16103-R), rabbit anti-mucin6 (1:200; LsBio, LS-C312108),  
652 rabbit anti-A4gnt (1:500, Novus Biologicals, NBP1-89129), rabbit anti-Gastrin (1:200, Leica  
653 Biosystems, NCL-GASp), mouse anti-MUC5AC (1:200; Leica Biosystems, NCL-HGM-45-M1),  
654 rabbit anti-vimentin (1:500; Abcam, ab92547), mouse anti-E-cadherin (1:200; BD  
655 Transduction Laboratories, 610181), mouse anti- $\beta$ -catenin (1:200; BD Transduction  
656 Laboratories, 610154), mouse anti-RFP (1:200; Abcam, 129244), mouse anti-ChgA (1:200;  
657 Abcam, 15160), rabbit anti-Phospho-MAPK (1:200; Cell Signalling, 4370S), mouse anti-H-K-  
658 ATPase (1:1,000; MBL International Corporation, D032-3), rabbit anti-Phospho-Akt (1:200;  
659 Cell Signalling, 3787L). Detailed information about clone number, and antibody validation is  
660 found in Supplementary Table 6. The peroxidase-conjugated secondary antibodies used were  
661 mouse/rabbit EnVision+ (DAKO) for HRP IHC or anti-chicken/rabbit/mouse Alexa  
662 488/568/647 IgG (1:500; Invitrogen) for IF. GSII-Lectin-AF568 (1:500, Thermofisher) was  
663 incubated on the slides for 1 hour at RT together with secondary antibodies. IHC sections  
664 were dehydrated, cleared, and mounted with DPX (Sigma) while IF sections were mounted in  
665 Hydromount (National Diagnostics) with Hoechst for nuclear staining. Immunostainings and  
666 imaging were performed on a minimum of three biological replicates and representative  
667 images of the replicates were included in the manuscript.

668 *Haematoxylin and eosin (H&E).*

669 H&E staining was performed on FFPE sections according to standard laboratory protocols.

670 *Whole mount analysis and vibratome sectioning*

671 Tissues were fixed in 4% paraformaldehyde/PBS (w/v) overnight at 4°C. Whole mount tissues  
672 were permeabilized in 2% TritonX-100/PBS (v/v) overnight at 4°C, while 500 µm vibratome  
673 sections were generated by sectioning tissues embedded in 4% low-melting point agarose  
674 with a vibrating microtome (Leica) and permeabilized in 2% TritonX-100/PBS (v/v) overnight  
675 at 4°C. Rapiclear (Sunjin lab) was used to clear whole mount tissues and vibratome sections  
676 according to manufacturer's instructions. Hoescht was used as nuclear counterstain.

#### 677 *In situ hybridization (ISH)*

678 ISH and co-ISH was performed using RNAscope<sup>45</sup> 2.5 High Definition Brown Assay and 2.5  
679 High Definition Duplex Reagent Assay (Advanced Cell Diagnostics) respectively, according to  
680 manufacturer's instructions. DapB was used as negative control for all the RNAscope  
681 experiments. *In situ* hybridization and imaging were performed on a minimum of three  
682 biological replicates and representative images of the replicates were included in the  
683 manuscript.

#### 684 *Analysis and scoring of stainings on mouse and human FFPE sections*

685 Overlap of Slc9a3-GFP and Aqp5-antibody stains was determined by counting stained cells  
686 contacting the lumen at the base of glands. The entire height of the gland base surrounding  
687 the gland base lumen had to be visible to avoid over-or underrepresentation of localized  
688 populations.

689 Samples of H&E sections of mouse gastric tumours were evaluated by qualified veterinary  
690 and clinical histopathologists. Scoring of AQP5 staining on human gastric cancer specimens  
691 was performed by qualified clinical histopathologists. The tumour in the tissue section was  
692 considered positive for AQP5 if staining was observed in more than 5% of the malignant cells.  
693 Subcellular localization of AQP5, relative staining intensities and stained features were all  
694 determined by qualified pathologists.

#### 695 **Microscopy imaging**

696 *Image acquisition*

697 IHC and H&E slides were imaged with Zeiss AxioImager Z1 Upright microscope. RNAscope  
698 slides and large area images were captured with Nikon Ni-E microscope/DS-Ri2 camera. IF  
699 slides were imaged using Olympus FV1000 and FV3000 confocal microscopes. Cultured  
700 organoids were imaged with Olympus DP-27 camera on Olympus IX53 inverted microscope.

701 *Image processing*

702 RNAscope and images with large areas were processed with NIS-Elements AR software  
703 (Nikon) with EDF and stitching features respectively. IF images were processed using ImageJ  
704 (NIH) and whole mount organoid images were processed using Imaris 8.0 (Bitplane).

705 **Statistics and reproducibility**

706 Gene expression data were quantified and depicted as the mean $\pm$ SEM. Statistical analyses  
707 were performed using GraphPad Prism. Data were tested for statistical significance by paired  
708 two-tailed *t*-test unless otherwise stated in figure legends. Statistical significance of overlap  
709 between the two gene sets in Fig. 1b was determined by hypergeometric distribution  
710 ([http://nemates.org/MA/progs/overlap\\_stats.html](http://nemates.org/MA/progs/overlap_stats.html)). Precise *P* values of statistical significance  
711 are shown in the respective figures. Representative images of all histological experiments and  
712 FACS sorting strategies were performed at least thrice independently with similar results,

713

714 **Supplementary References**

- 715 38. Madisen, L. *et al.* A robust and high-throughput Cre reporting and characterization  
716 system for the whole mouse brain. *Nat. Neurosci.* **13**, 133–140 (2010).
- 717 39. Jackson, E. L. *et al.* Analysis of lung tumor initiation and progression using conditional  
718 expression of oncogenic K-ras. *Genes Dev.* (2001). doi:10.1101/gad.943001
- 719 40. Shibata, H. *et al.* Rapid colorectal adenoma formation initiated by conditional targeting  
720 of the APC gene. *Science (80-. )*. (1997). doi:10.1126/science.278.5335.120

- 721 41. Suzuki, A. *et al.* T cell-specific loss of Pten leads to defects in central and peripheral  
722 tolerance. *Immunity* (2001). doi:10.1016/S1074-7613(01)00134-0
- 723 42. Leushacke, M. *et al.* Lgr5-expressing chief cells drive epithelial regeneration and  
724 cancer in the oxyntic stomach. *Nat Cell Biol* **19**, 774–786 (2017).
- 725 43. Monaco, G. *et al.* RNA-Seq Signatures Normalized by mRNA Abundance Allow  
726 Absolute Deconvolution of Human Immune Cell Types. *Cell Rep.* (2019).  
727 doi:10.1016/j.celrep.2019.01.041
- 728 44. Mi, H., Muruganujan, A., Casagrande, J. T. & Thomas, P. D. Large-scale gene  
729 function analysis with the panther classification system. *Nat. Protoc.* (2013).  
730 doi:10.1038/nprot.2013.092
- 731 45. Wang, F. *et al.* RNAscope: A novel in situ RNA analysis platform for formalin-fixed,  
732 paraffin-embedded tissues. *J. Mol. Diagnostics* (2012).  
733 doi:10.1016/j.jmoldx.2011.08.00
- 734 46. Subramanian, A. *et al.* Gene set enrichment analysis: A knowledge-based approach  
735 for interpreting genome-wide expression profiles. *Proc. Natl. Acad. Sci. U. S. A.*  
736 (2005). doi:10.1073/pnas.0506580102
- 737 47. Mootha, V. K. *et al.* PGC-1 $\alpha$ -responsive genes involved in oxidative phosphorylation  
738 are coordinately downregulated in human diabetes. *Nat. Genet.* (2003).  
739 doi:10.1038/ng1180
- 740

741 **Acknowledgements**

742 The authors would like to thank staff at the IMB-IMU and the SBIC-Nikon Imaging Centre for  
743 imaging assistance, the research coordination team and Department of Pathology at NUH for  
744 assistance with human samples. They also thank Sowmya Sagiraju (A\*Star IMB) for  
745 assistance with animal experiments, Adelia Lin (A\*Star IMB) and Annie Ng (A\*Star IMB) with  
746 empirical candidate validation, Kikue Saito (Kanazawa Medical University) for assistance with  
747 RNA-SEQ preparation, Makoto Taniguchi (Kanazawa Medical University) and Kenji Kita  
748 (Kanazawa University) for assistance with FACS sorting. D. H. Alpers (Washington  
749 University School of Medicine) for providing the Gastric Intrinsic Factor antibody, Alexander  
750 van Oudenaarden and Anna Lyubimova (Hubrecht Institute) for assistance with CEL-Seq and  
751 RaceID, and Fred de Sauvage (Genentech) for providing the Lgr5-DTR-EGFP mice. S.H.T. is  
752 supported by the National Medical Research Council (NMRC) Singapore  
753 (NMRC/OFYIRG/0007/2016). N.B. is supported by the Agency for Science, Technology and  
754 Research (A\*Star), Singapore Gastric Cancer Consortium (SGCC) and Japan Society for the  
755 Promotion of Science (JSPS). This research was also supported by the National Research  
756 Foundation, Prime Minister's Office, Singapore under its Investigatorship Program (Award No.  
757 NRF-NRF12017-03).

758

759 **Author Information**

760 All correspondence and requests for materials should be addressed to Nick Barker  
761 ([Nicholas.barker@imb.a-star.edu.sg](mailto:Nicholas.barker@imb.a-star.edu.sg)).

762

763 **Ethics Declaration**

764 The authors declare the following competing interest:

765 N.B. and S.H.T. are co-inventors of the provisional patent application 10201911742W titled "A  
766 method for functional classification and diagnosis of cancers". This patent covers the analysis  
767 of human cancers using their signalling pathway statuses.

768 All the other authors declare no competing interest.

769

#### 770 **Author contributions**

771 S.H.T and Y.S. contributed to all aspects of the study – they designed, performed all empirical  
772 experiments, collected, analyzed data and wrote the manuscript. Y.S. designed, performed  
773 experiments, collected and analyzed data for profiling and validation studies for candidate  
774 marker identification. J.G. performed immunostaining, CEL-Seq experiments, mouse  
775 husbandry. R.S. provided advice and technical help with human and mouse cancer, analysed  
776 data and wrote the manuscript. K.M. performed FACS and immunostaining for human AQP5-  
777 FACS experiments. P.P. performed immunostaining and mouse husbandry. L.T.T. performed  
778 mouse husbandry. E.W. generated the transgenic mouse lines. T.S., S.W.T.H., analysed  
779 human cancer data in pathway analysis. S.L.I.J.D. analysed microarray, CEL-Seq and  
780 RNASEQ data. S.M. performed FACS experiments. A.F. provided advice and technical help  
781 with human experiments and mouse cancer models. M.O. T.T., H.G., S.S., T.M., K.G.Y., J.S.  
782 and A.S. provided patient samples. H.G, S.S. and T.M. analysed and scored stained patient  
783 samples. P.T. designed and supervised cancer frequency analysis. N.B. supervised the  
784 project, analyzed the data and wrote the manuscript. All authors discussed results and edited  
785 the manuscript.

786

#### 787 **Data and code availability**

788 Microarray data that support the findings of this study have been deposited in the Gene  
789 Expression Omnibus (GEO) under accession code GSE121803. RNASEQ data of AQP5+  
790 and AQP5- human samples have also been deposited in the Gene Expression Omnibus  
791 (GEO) under accession code GSE133036. Source data for Figs. 1-4 and Extended Data Figs.  
792 1, 2, 4-6, 9 are provided with the paper. Any other relevant data supporting the findings of this  
793 study are available from the corresponding author on reasonable request.

794

795 **Extended Data Figure Legends**

796 Extended Data Fig. 1

797 (a-c) FACS sorting strategy sorting GFP<sup>hi</sup> and GFP<sup>lo</sup> cells from Lgr5-EGFP-IRES-CreERT2  
798 pylorus (a), small intestine (b) and colon (c).

799 (d) *Lgr5* expression (qPCR) in sorted populations and unsorted tissues of the gastrointestinal  
800 tract data represented as means± s.e.m. (n=4 biological replicates); one-way ANOVA test.

801 (e) *Aqp5* protein expression in the mouse stomach through to the duodenum by  
802 immunostaining (n=3 biological replicates).

803 (f-i) *Aqp5* mRNA expression in the corpus (f), Brunner's glands (g), small intestine (h) and  
804 colon (i) by ISH (n=3 biological replicates).

805 (j-n) *A4gnt* (j), *GIF* (k), *Muc6* (l), *Slc9a3* (m) and *Spp1* (n) expression in the corpus, Brunner's  
806 glands, small intestine and colon by qPCR, ISH, and co-ISH with *Lgr5*. For histology  
807 experiments, n=3; For qPCR, n=4 biological replicates for *GIF*, *Muc6* and *Slc9a3* qPCRs  
808 where data is represented as means± s.e.m., n=2 technical replicates from a pooled sample  
809 of 8 for *A4gnt* and *Spp1* qPCRs.

810 Scale bars represent 500 µm in (e), and 20 µm in (f-n).

811

812 Extended Data Fig. 2

813 (a) Exon1-knockin gene strategy to generate EGFP-CreERT2 reporters of *Aqp5*, *A4gnt*,  
814 *Slc9a3* and *Spp1* expression.

815 (b) 3'UTR-knockin gene strategy to generate 2A-EGFP, 2A-CreERT2 or 2A-DTR reporters of  
816 *Aqp5*, *Slc9a3* and *Lgr5* expression.

817 (c-f) GFP signal in the pylorus and small intestine of *Aqp5*-2A-EGFP (c-d) and *Slc9a3*-2A-  
818 EGFP mice (e-f).

819 (g-h) Quantification of the overlap between *Slc9a3*-2A-EGFP<sup>+</sup> cells and *Aqp5*<sup>+</sup> cells (g)  
820 (n=102 glands from three mice) and a representative image of the immunostaining (h). Results  
821 are presented as means±s.e.m.

822 (i-j) Quantification of overlap between Lgr5-EGFP+ cells with Aqp5+ cells (i) (n=117 glands  
823 from four mice) and a representative image of the immunostaining (j). Results are presented  
824 as means±s.e.m.  
825 (k-m) Co-localization of Lgr5-EGFP in the pylorus with GIF (k), Gastrin (l) and Chromogranin  
826 A (m) (n=3 biological replicates).  
827 (n) t-SNE map of single Lgr5<sup>Hi</sup> cells from the pylorus (n=285 cells from three mice).  
828 (o-s) t-SNE maps showing enrichment of candidate markers in major (o-q) and minor (r-s)  
829 subpopulations of Lgr5<sup>Hi</sup> pyloric cells (n=285 cells from 3 mice).  
830 (t) Frequency of 10 published proliferation markers (*Bcl2*, *Ccnd1*, *Ckap2*, *Foxm1*, *Ki67*, *Mcm2*,  
831 *Mybl2*, *Plk1*, *Rrm2*, *Top2a*) in major versus minor subpopulations, compared by two-tailed  
832 Mann-Whitney test (n=285 cells from 3 mice, 248 cells in major, 8 cells in minor 1 and 1 cells  
833 in minor 2 populations).  
834 (u-v) *Aqp5* (u) and *Lgr5* (v) expression in cells sorted from Aqp5-EGFP-IRES-CreERT2 pylori  
835 (means±s.e.m.; n= 4 biological replicates).  
836 (w-x) Co-immunostaining for EGFP driven by Aqp5-EGFP-IRES-CreERT2 and endogenous  
837 Aqp5 (w) and Ki67 (x) (n=3 mice).  
838 Scale bars represent 50 µm in (g),(h) and 25 µm in (k),(m),(w),(x).

839

#### 840 Extended Data Fig. 3

841 (a-p) Lineage tracing in A4gnt-, Aqp5-, Spp1- and Slc9a3-EGFP-IRES-CreERT2 mice crossed  
842 with tdTomato<sup>LSL</sup> reporter mice after short trace (20-48 hours) in the pylorus (a-d) and small  
843 intestine (i-l) and long trace (>3 months) in the pylorus (e-h) and small intestine (m-p) (n=3 per  
844 genotype).  
845 (q-x) Lineage tracing in pylorus (q-t) and small intestine (u-x) of the Aqp5-2A-CreERT2 and  
846 Slc9a3-2A-CreERT2 mice after short trace (q-r, u-v) and long trace (s-t, w-x).  
847 (y-b') Whole-mount imaging of pylorus from induced Aqp5-EGFP-IRES-CreERT2;tdTomato<sup>LSL</sup>  
848 mice 20 hours (y) and 6 months (z) after induction. Whole-mount imaging of pylorus from  
849 uninduced 8 week-old (a') and 8 month-old (b') Aqp5-EGFP-IRES-CreERT2;tdTomato<sup>LSL</sup> mice

850 (n=3 per condition). dTom signal through the entire height of the pyloric epithelium is shown  
851 and DAPI from the upper parts of pyloric glands is depicted for clarity.  
852 (c'-e') dTom signal in clusters of glands in 1 year-traced pylorus (c') and small intestine (d'-e').  
853 (f'-h') dTom expression in gastric corpus (f'), colon (g') and brunner's glands (h') 20 h and 6  
854 months after induction.  
855 N=3 biological replicates. Scale bars represent 50  $\mu$ m.

856

857 Extended Data Fig. 4

858 (a) Aqp5+ gating strategy with cells from WT pylorus stained only with propidium iodide.  
859 (b) Heatmap of transcriptomes from Aqp5+ and Aqp5- cells (n=4 biological replicates).  
860 (c) GSEA analysis comparing degree of overlap between transcriptomes of Aqp5+ cells and  
861 Lgr5+ cells from the pylorus using Kolmogorov-Smirnov statistic (n=4 biological replicates  
862 each).  
863 (d-e) Relative *Aqp5* (d) and *Lgr5* (e) expression (from microarray) in Aqp5+ and Aqp5- cells  
864 (n=4 biological replicates) by one-way ANOVA in Partek suite.  
865 (f-h) Relative expression of various pyloric markers (f), other published pyloric stem cell  
866 markers (g) and lineage and proliferation markers (h) in Aqp5+ population versus Aqp5-  
867 population in microarray (n=4 biological replicates). Data represented as means, as derived  
868 from Partek Analysis Software by one-way ANOVA.  
869 (i-j) Aqp5 staining in a whole-mount organoid (i) and Aqp5 co-localization with Ki67 (j) in an  
870 organoid section. Organoids were derived from single Aqp5+ cells (n=3 biological replicates).  
871 (k-r) Pylori of DT-treated WT (k-n) and Aqp5-2A-DTR (o-r) mice stained for H&E (k, o), E-  
872 Cadherin (l, p), Gif (m, q) and Gastrin (n, r) (n=3 biological replicates).  
873 (s-u) Outgrowth efficiency of Aqp5+, Aqp5-, Lgr5-EGFP+, Lgr5-EGFP- cells (s) (n=5 biological  
874 replicates for Aqp5+/- cells, n=3 biological replicates for Lgr5-EGFP+/- cells). Representative  
875 images of organoids derived from Lgr5-EGFP+ (t) and Lgr5-EGFP- (u) cells. Paired two-sided  
876 t-test.  
877 Scale bars represent 25  $\mu$ m in (i-j), 50  $\mu$ m in (k) to (r), and 500  $\mu$ m in (t) and (u).

878

879 Extended Data Fig. 5

880 (a-f') *MUC6* (a-b'), *A4GNT* (c-d') and *SLC9A3* (e-f') expression (co-ISH with *LGR5* and  
881 immunostaining) in normal human pylorus (n=3 biological replicates).

882 (g-j) Co-ISH to co-localize *AQP5* with *PEPC* (g), *MUC6* (h), *GIF* (i) and *MUC5AC* (j) pyloric  
883 lineage markers (n=3 biological replicates).

884 (k-l) *AQP5* labelling in whole mount human organoids (k) and *AQP5* colocalization with KI67  
885 (l) in organoid sections (n=3 biological replicates).

886 (m-o) Relative *AXIN2* (m), *TFF2* (n) and *AQP5* (o) expression in *AQP5*+ cell-derived organoids  
887 3 days after WNT3A, Noggin and FGF10 withdrawal by qPCR (n=3 biological replicates).

888 Scale bars represent 100  $\mu\text{m}$  in all panels except (a'), (b'), (c'), (d'), (e'), (f'), (k) where they  
889 represent 25  $\mu\text{m}$ .

890

891 Extended Data Fig. 6

892 (a-e) qPCR validation (green, n=5 biological replicates) and RNASEQ values (blue, n=8  
893 biological replicates) of murine stem cell markers (a), membrane components (b), chemokine  
894 signaling components (c), extracellular matrix components (d) and other genes (e). Two-sided  
895 Mann-Whitney test was used to determine statistical significance of qPCR results differences  
896 for all genes except *AQP5*, which was determined by two-tail paired t-test. qPCR and  
897 RNASEQ results are presented as means.

898 (f-f'') ISH of *SMOC2* (brown) on normal human pylorus. (f) is magnified inset of surface  
899 mucosa, while (f') is magnified inset of gland base (n=4 biological replicates). Scale bars  
900 represent 100  $\mu\text{m}$  in (f), and 10  $\mu\text{m}$  in (f') and (f'').

901 (g) Top 10 Panther pathways enriched with most candidate genes.

902

903 Extended Data Fig. 7

904 (a-b) Co-hyperactivation status of the Wnt, PI3K and Kras pathways in human distal gastric  
905 cancer samples from TCGA<sup>3</sup> (a) (n=155) and GSE15459<sup>16</sup> (b) (n=42) datasets. Heatmaps

906 show distribution of pathway hyperactivation statuses across samples. Graphs depict  
907 distribution of  $\mu$ -scores (degree of signalling activity) of normal and tumour samples for each  
908 of the pathways examined.

909

910 Extended Data Fig. 8

911 (a) Sample sizes, tumour and invasion incidences observed in various permutations of  
912 CreERT2 drivers and oncogenic alleles.

913 (b-g) Whole mount and H&E images of entire pyloric regions for each CreERT2-oncogenic  
914 allele combination.

915 (h-l) H&E images of pylori from multiple pyloric marker-CreERT2;Kras<sup>LSL-G12D</sup> models (h-i),  
916 APK-only model (without CreERT2 driver) (j), and small intestine (k) and colon (l) from Aqp5-  
917 IRES-CreERT2;APK gastric cancer mouse model.

918 Scale bars represent 1 cm in whole mount insets in (b-g), 200  $\mu$ m in H&E images in (b-l).

919

920 Extended Data Fig. 9

921 (a-g) Immunostaining of various markers in Aqp5-IRES-CreERT2;APK pyloric tumour.

922 (h-h'') Co-ISH of Aqp5 and Lgr5 in tumour region, magnified in (h'). Dual ISH of Aqp5 and Lgr5  
923 in an adjacent normal pyloric region from the same mouse (h'').

924 (i-i') Representative H&E stain of a salivary gland tumour from Aqp5-IRES-CreERT2;APK  
925 mouse.

926 (j-o) Immunostaining of various markers in Slc9a3-2A-CreERT2;AP pyloric tumour.

927 (p-w) Immunostaining of various markers in the APK-only (no CreERT2) control pyloric  
928 stomach.

929 (x-x') Colocalization of Aqp5-EGFP and endogenous Aqp5 protein in pyloric tumour from an  
930 Aqp5-IRES-CreERT2;APK mouse.

931 (y-z) Control FACS gating for GFP+ cells using normal Aqp5-EGFP-IRES-CreERT2 (y) and  
932 WT (z) pylori (n=3 biological replicates).

933 (y-z'') Organoid assay for stemness of Aqp5-GFP+ tumour cells (n=3 biological replicates). (y)  
934 Experimental timeline. FACS gating strategy to isolate GFP+ tumour cells from Aqp5-  
935 CreERT2;APK pyloric tumour (z), GFP+ cells from normal Aqp5-EGFP-IRES-CreERT2  
936 pylorus (z'), and control GFP gating with WT pylorus (z'').  
937 Scale bars represent 100  $\mu$ m in (a-g and i-x'), 100  $\mu$ m in (h'), 20  $\mu$ m in (h'').

938 Extended Data Fig. 10

939 (a) Summary of AQP5 expression in a tumour microarray panel of 145 cores of human distal  
940 gastric cancer. AQP5 expression is scored as positive if observed in > 5% malignant cells.  
941 (b-e) Examples of AQP5+ cores with intestinal (b-c) and diffuse (d-e) subtypes, often with  
942 cytoplasmic and/or membranous staining.  
943 (f) Summary of AQP5 expression from 54 full sections of distal human gastric cancer.  
944 (g-n) AQP5 expression in intestinal (g),(h),(k),(l) and diffuse (l),(j),(m),(n) subtypes. Yellow  
945 arrowheads indicate cells co-expressing AQP5 and KI67.  
946 (o) Summary of other observations of AQP5 expression in full gastric tumour sections.  
947 (p-s) AQP5 expression in the invasive edge of the tumour (p), intestinal metaplasia (IM) (q,  
948 dotted lines denote IM region negative for AQP5), Signet ring cells (r, black arrows denote  
949 cells with weak AQP5 expression) and tumour cells in lymph node (LN) metastasis (s).  
950 \*Mixed refers to AQP5 localization in cytoplasm and nucleus, or cytoplasm and membrane.  
951 Scale bars represent 20  $\mu$ m in (g-n), (q-r), 50  $\mu$ m in (b-e), (p), (s).

952 **Supplementary information** is available for this paper.

953 Peer review information.

954 Reprints and permissions information is available at [www.nature.com/reprints](http://www.nature.com/reprints).

**Fig. 1**

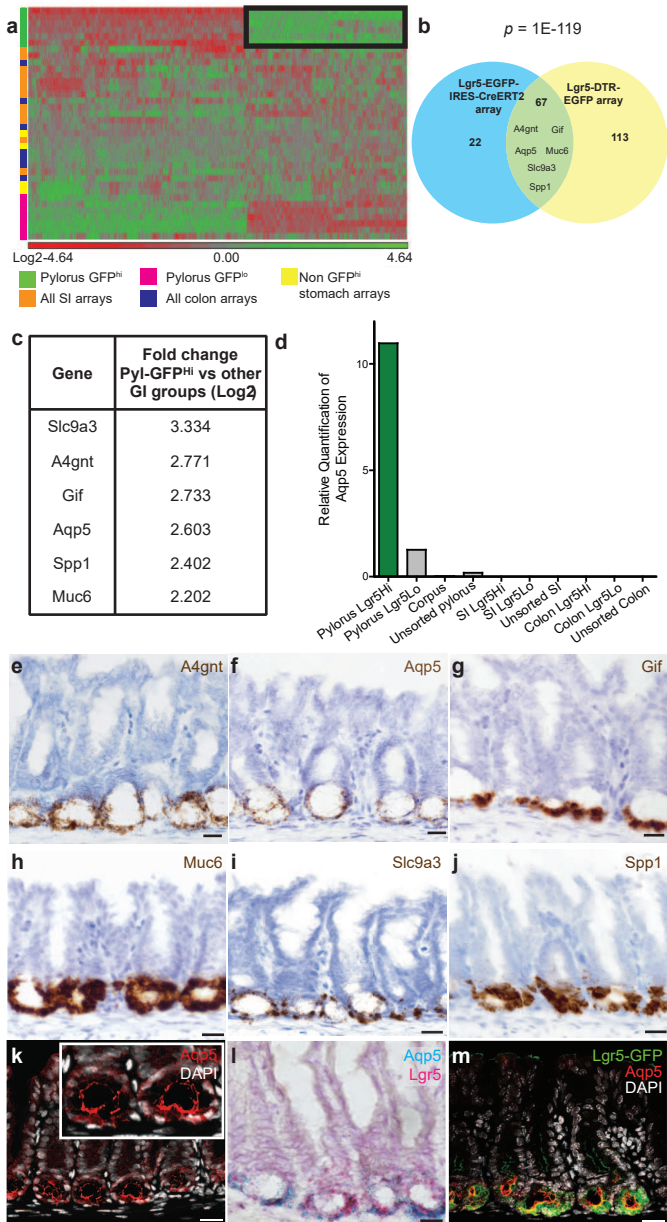


**Fig. 2**

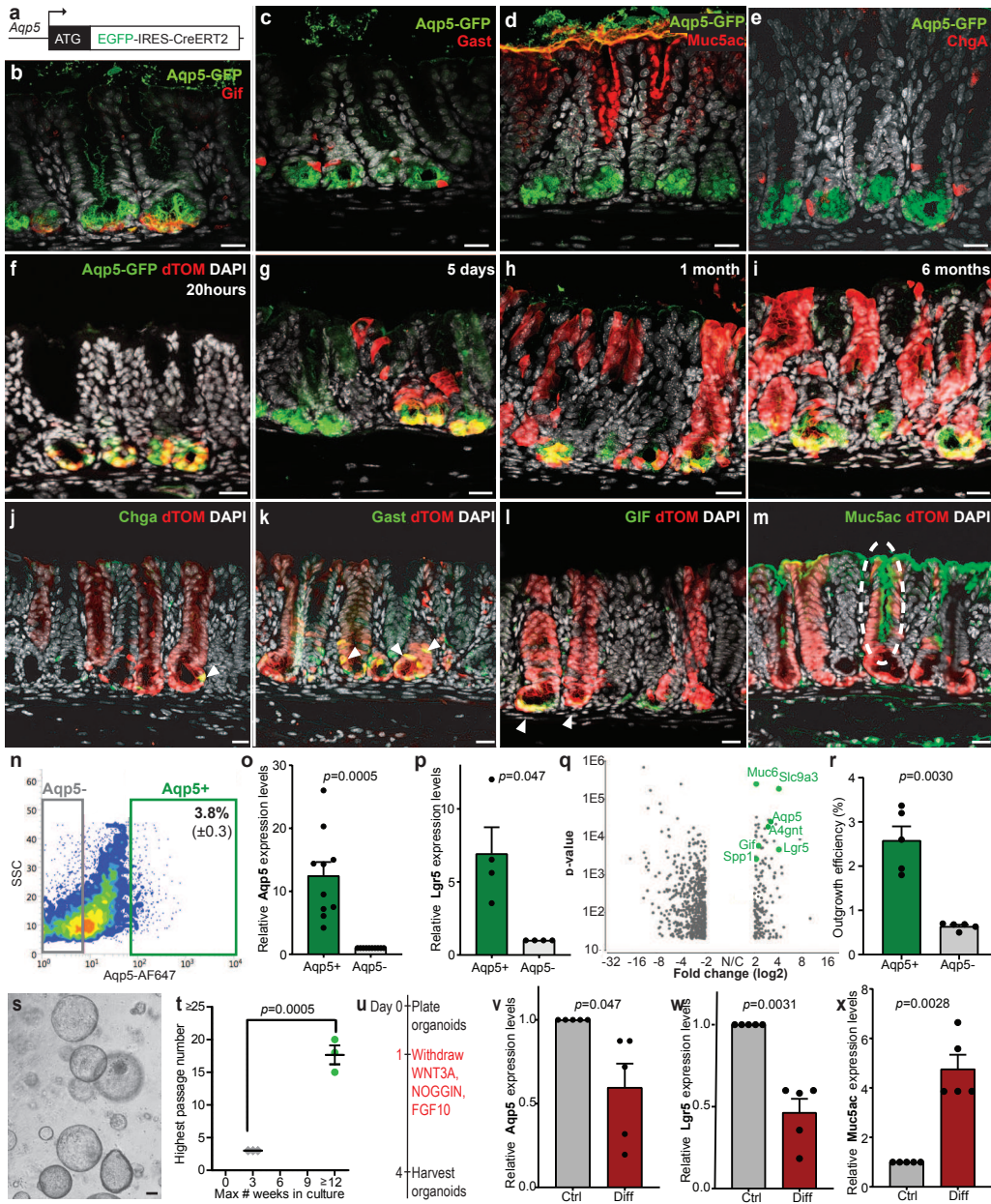


**Fig. 3**

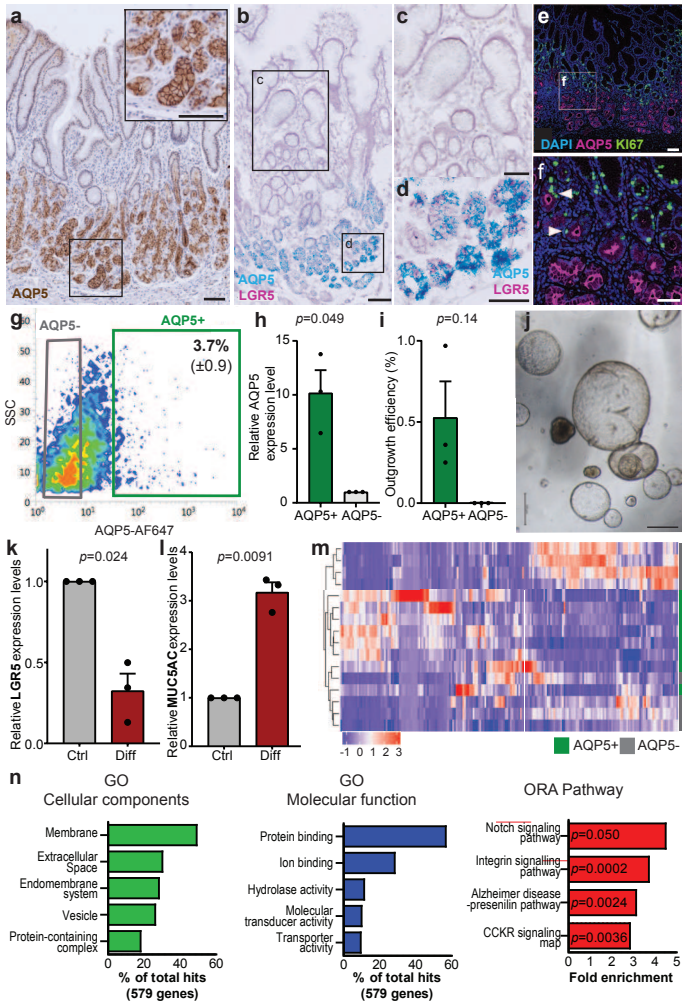
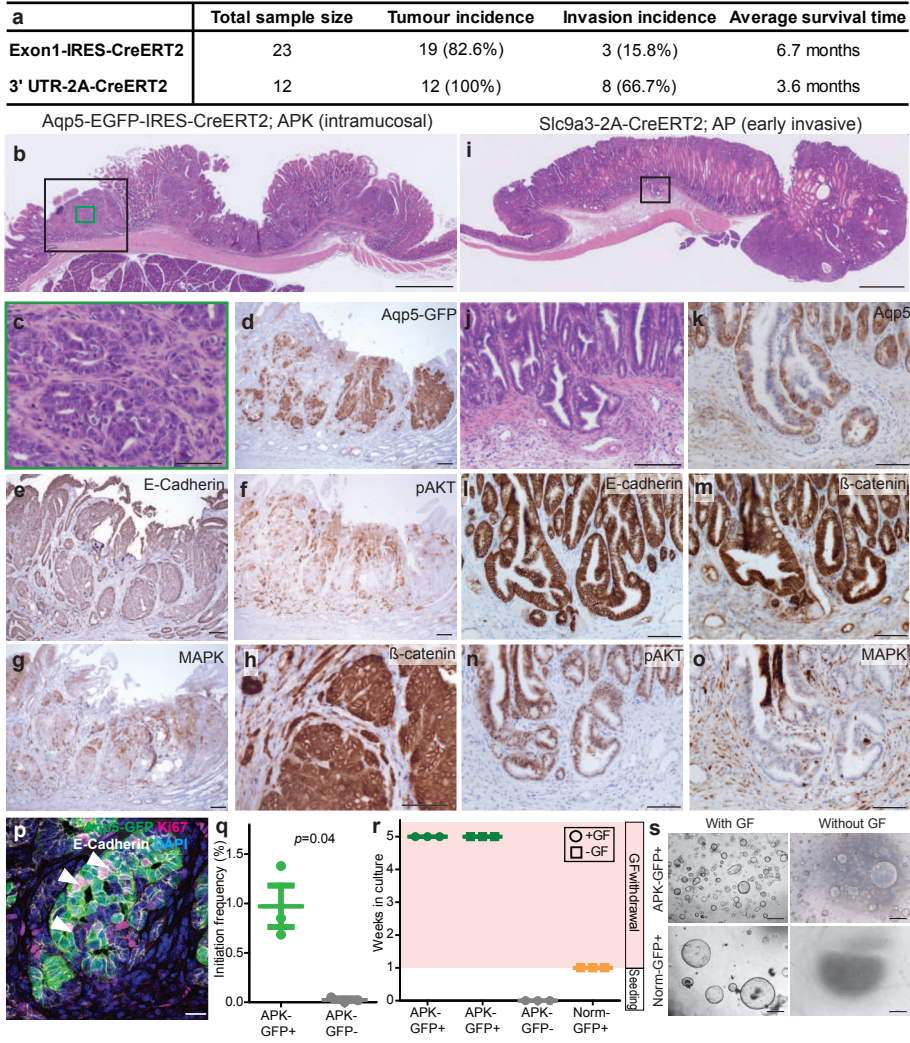
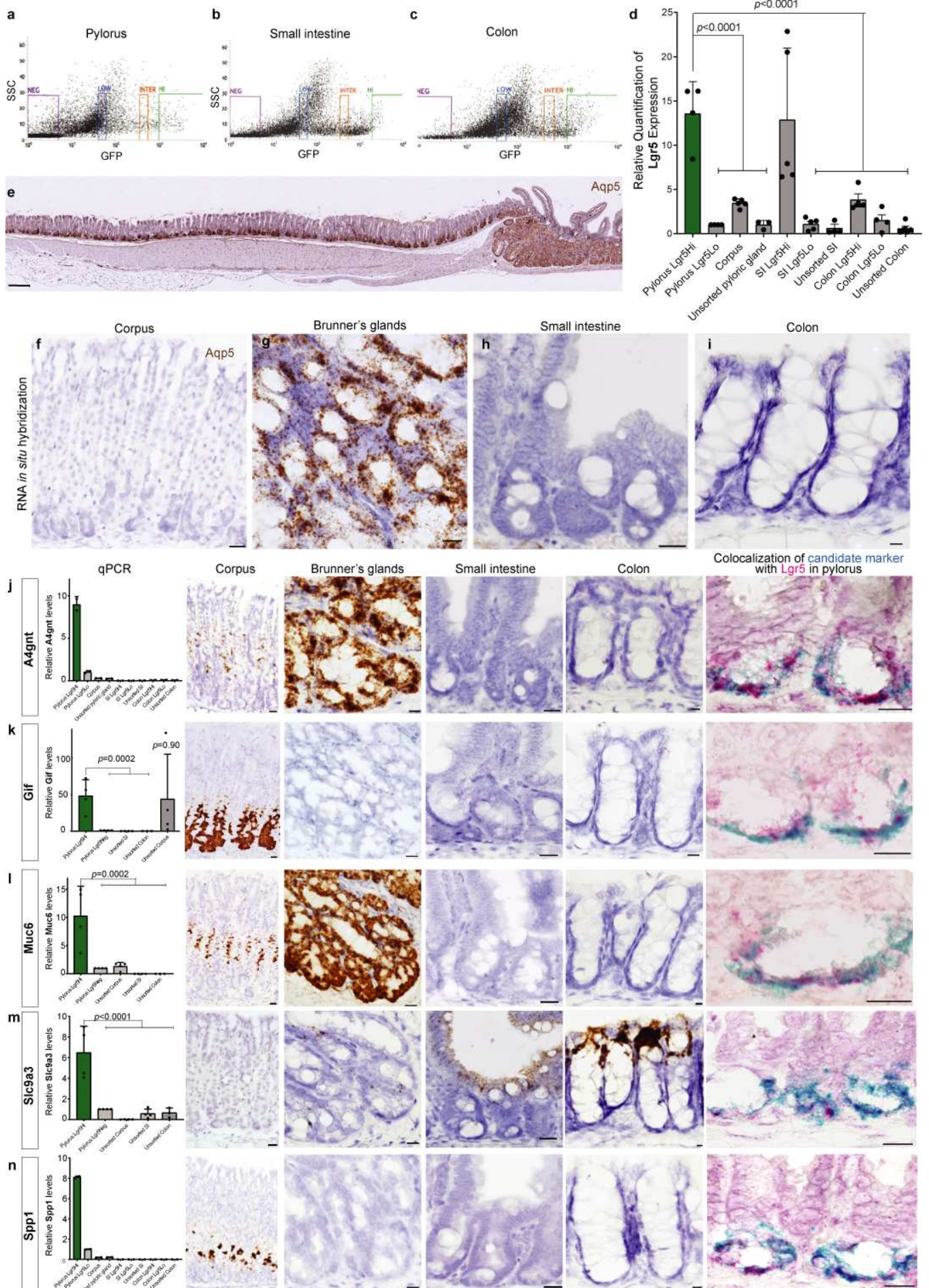


**Fig. 4**

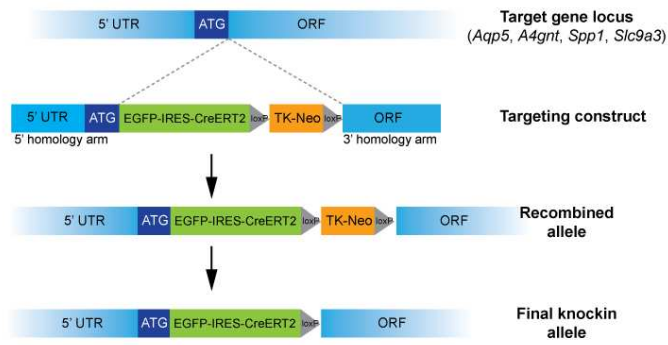


# Extended Data Fig. 1

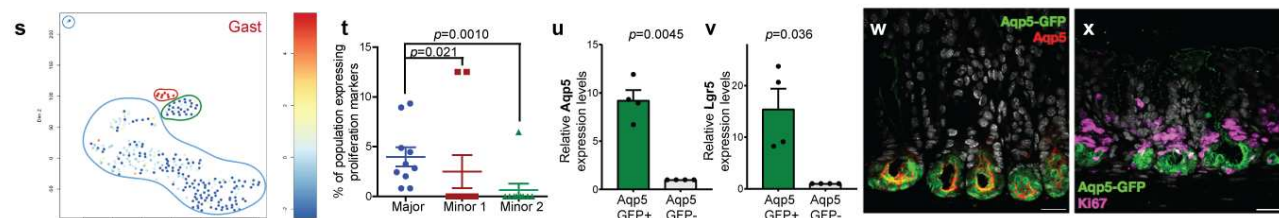
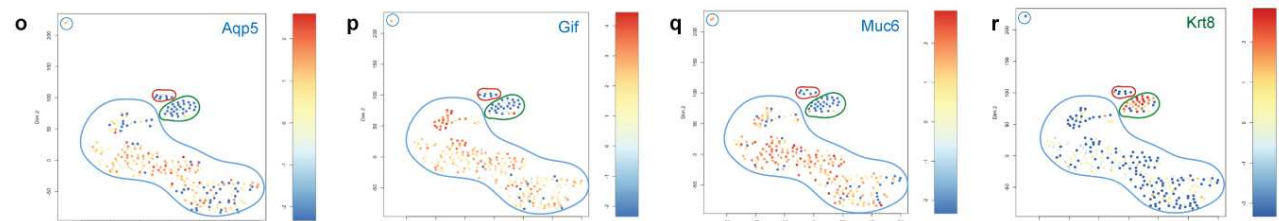
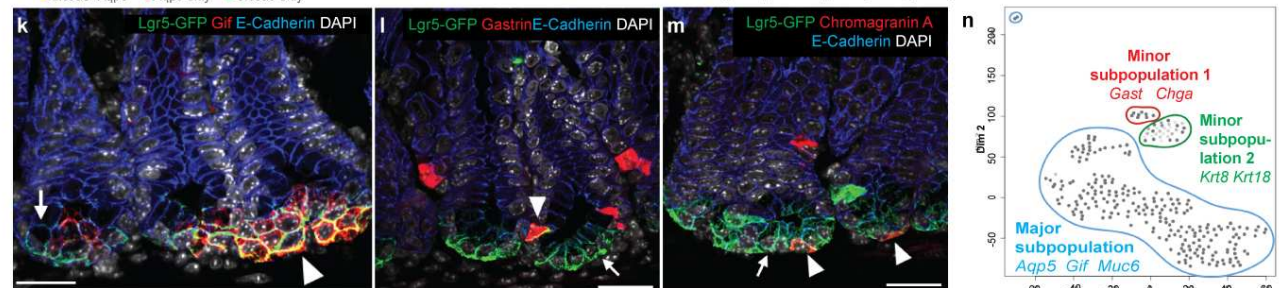
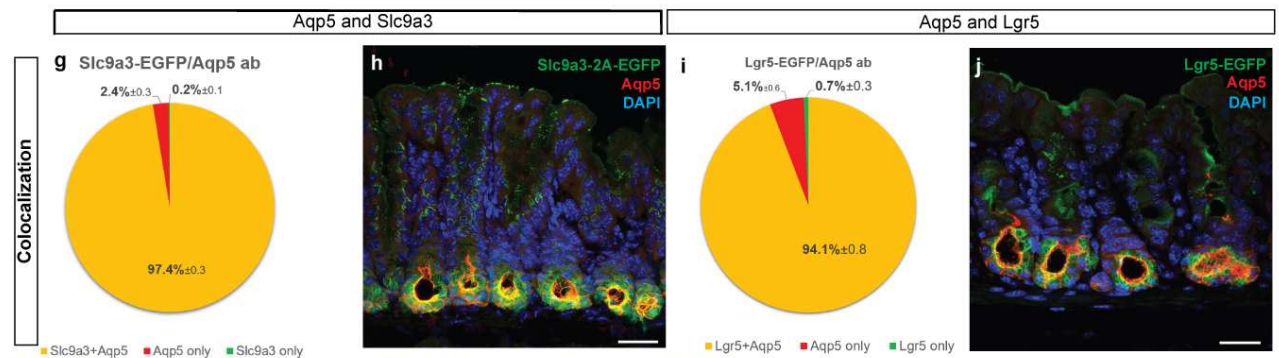
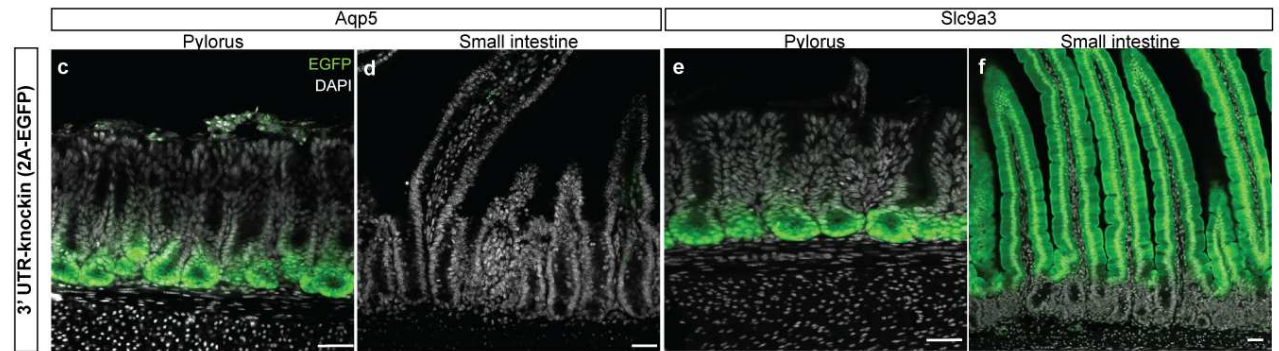
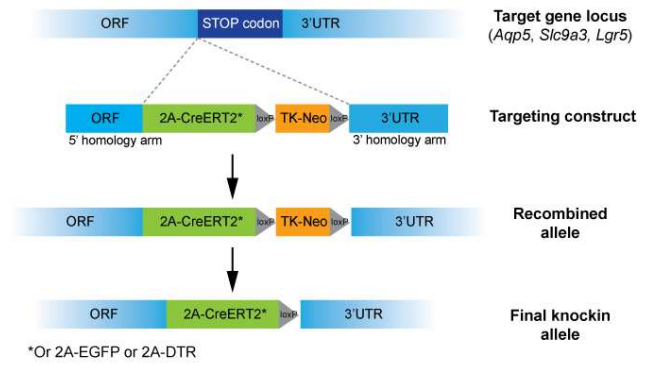


## Extended Data Fig. 2

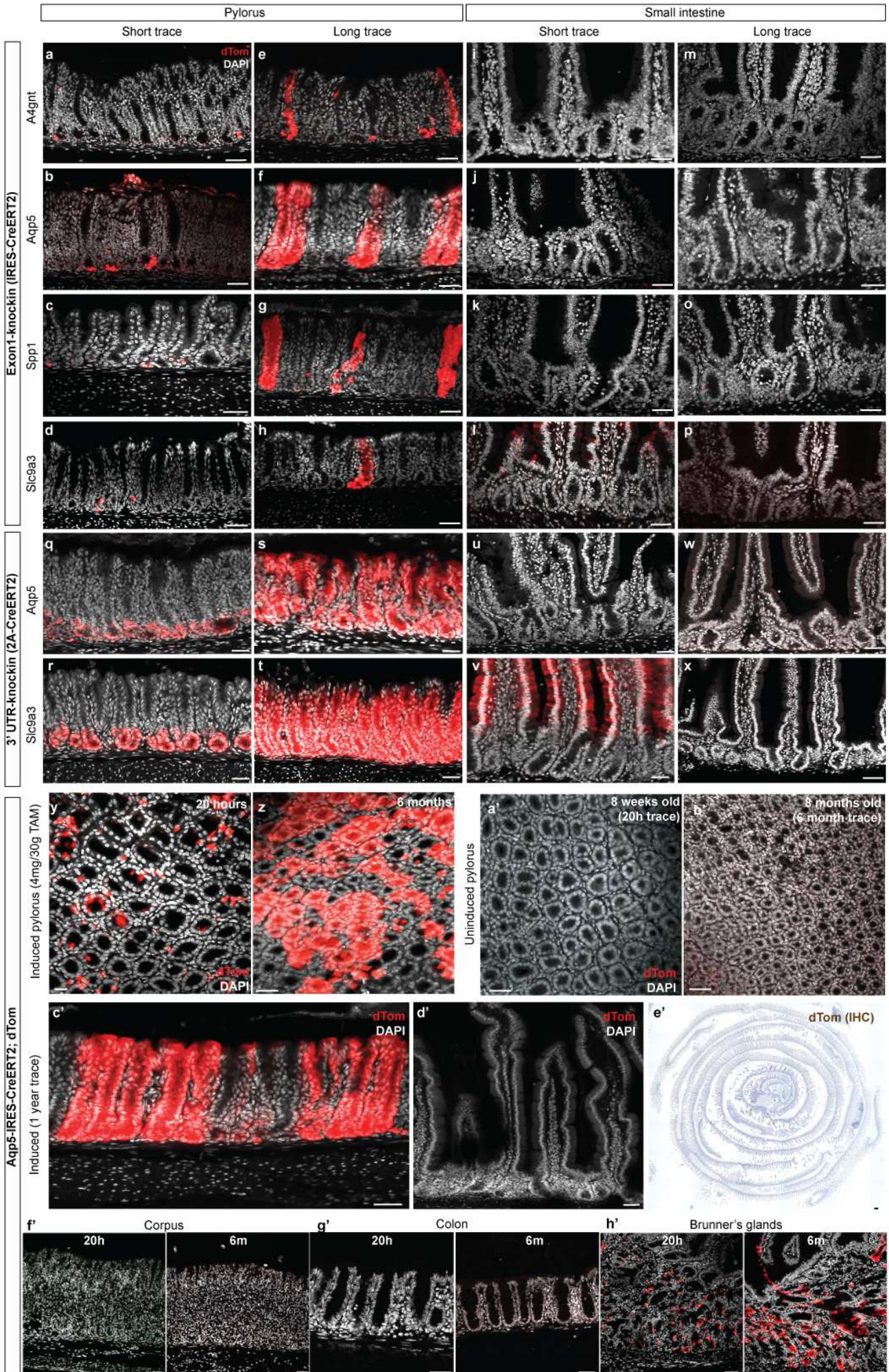
### a Targeting strategy for EGFP-IRES-CreERT2 construct



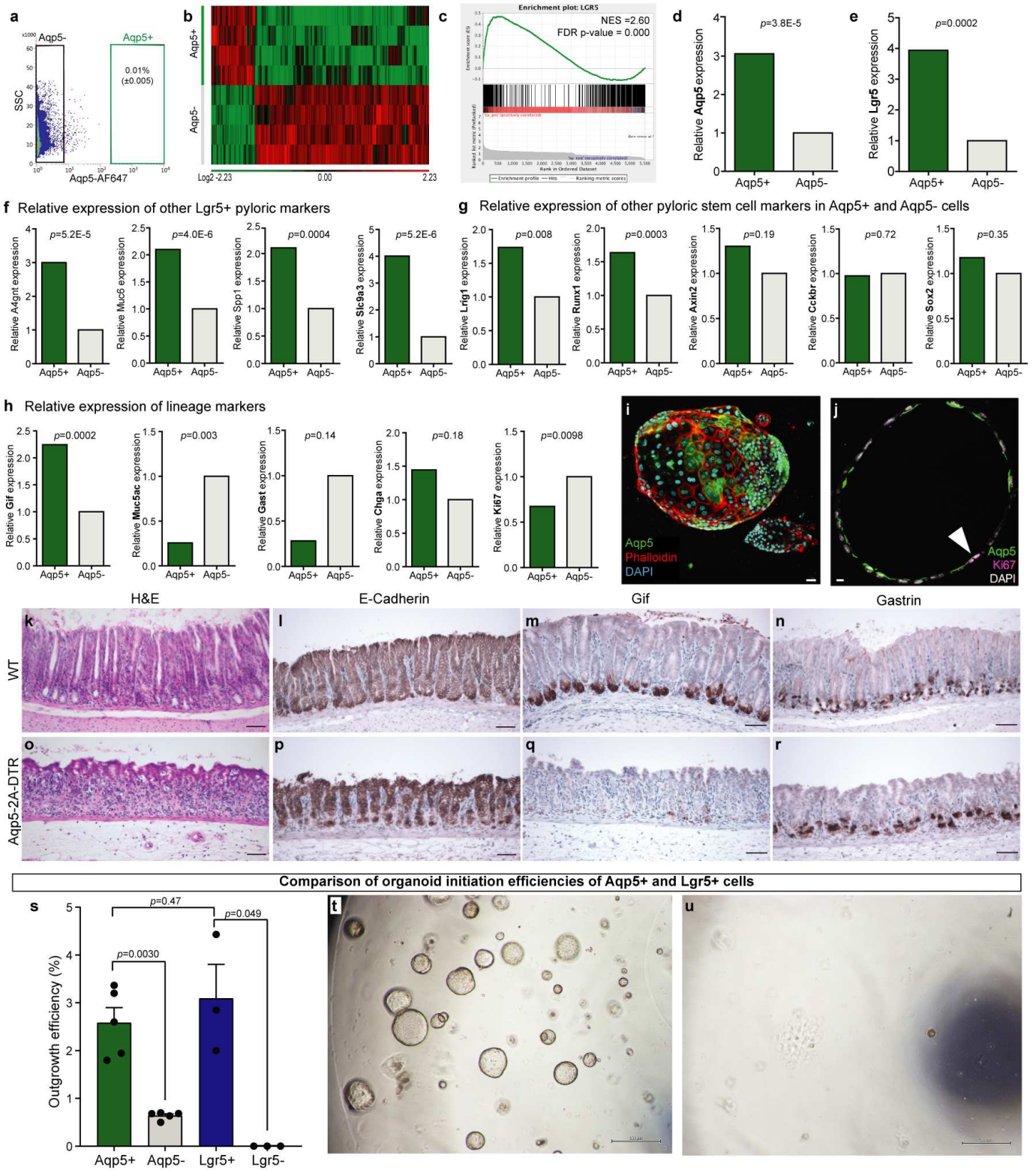
### b Targeting strategy for 2A-CreERT2, 2A-EGFP and 2A-DTR constructs



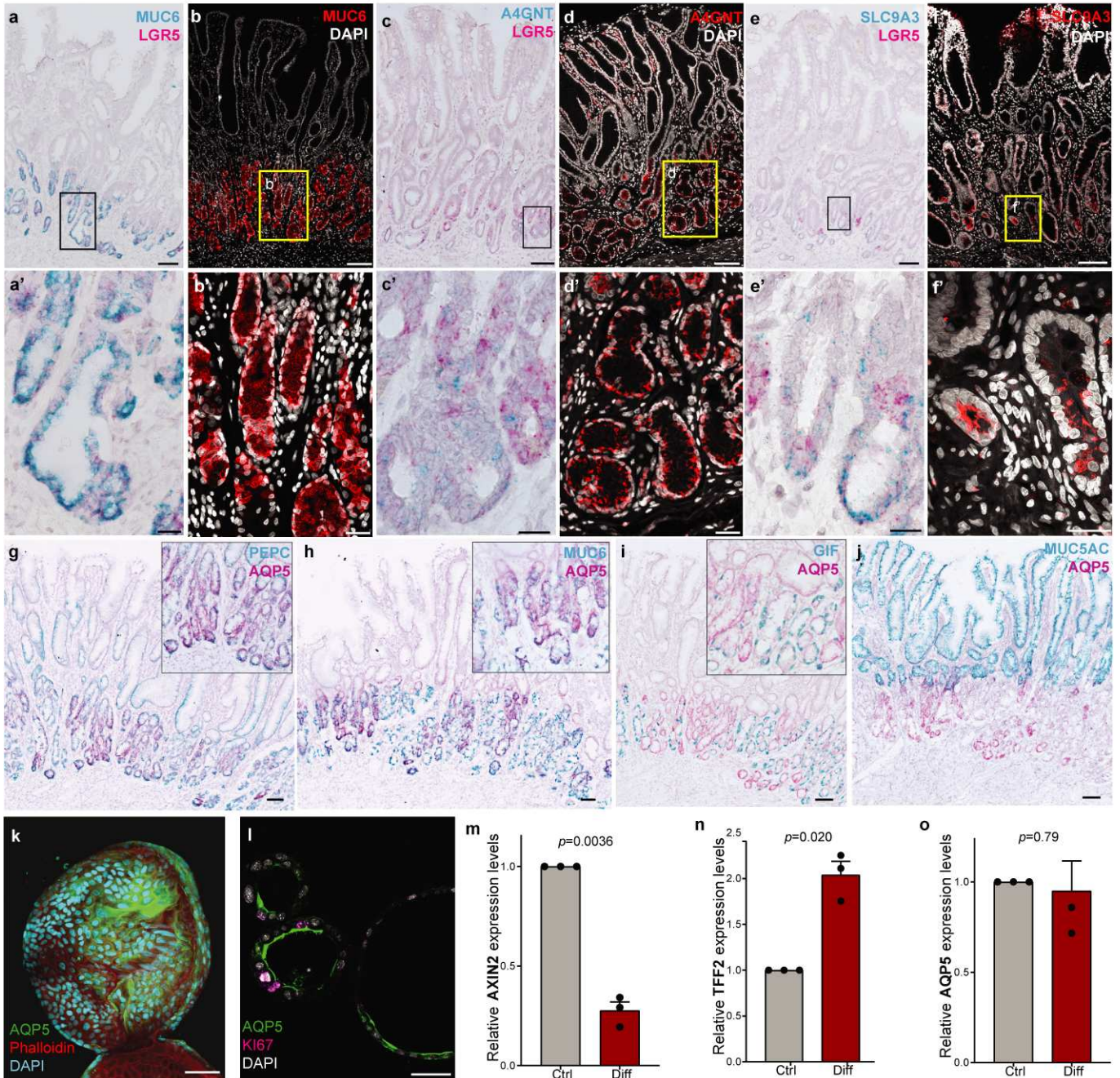
Extended Data Fig. 3



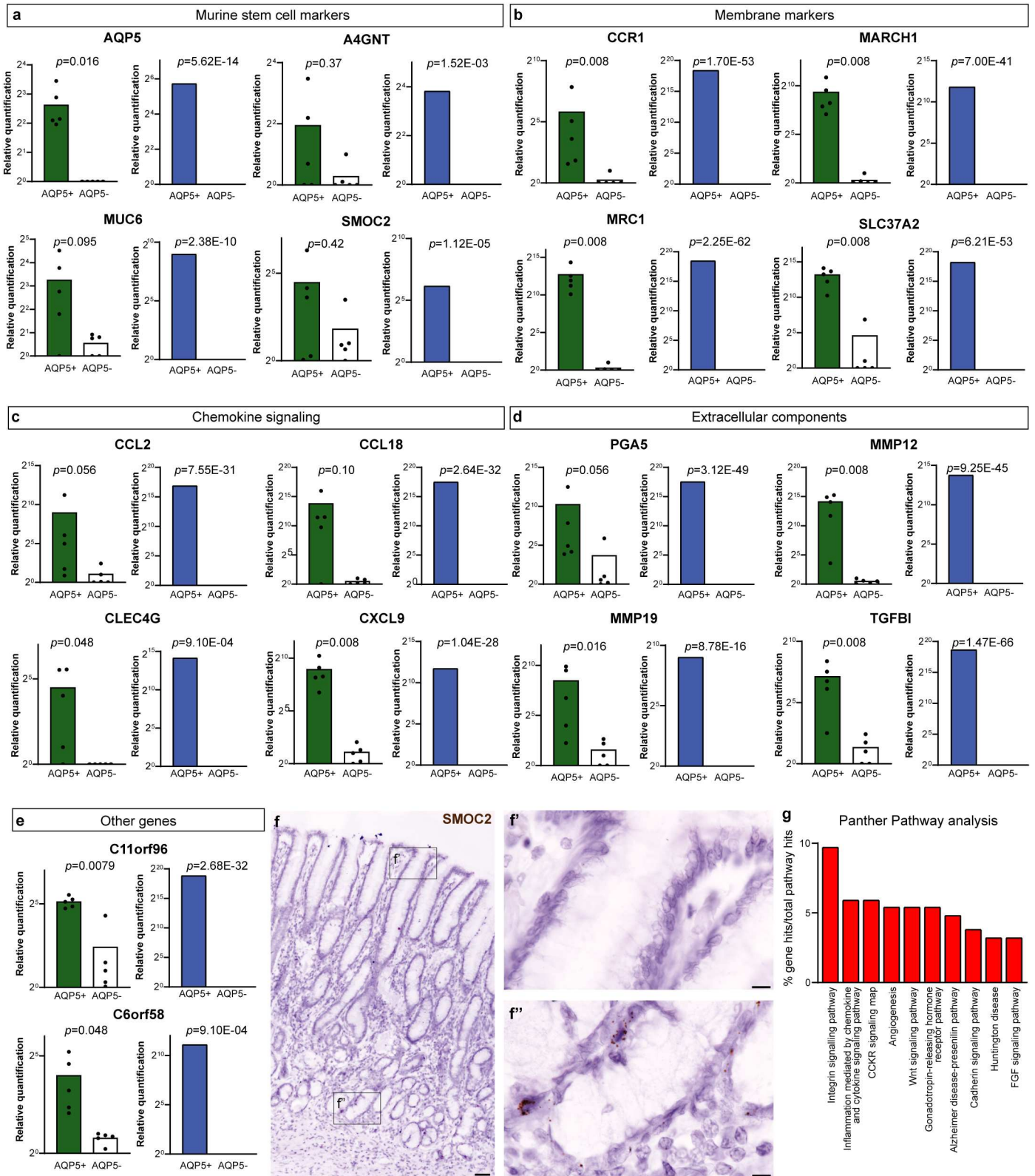
## Extended Data Fig. 4



Extended Data Fig. 5



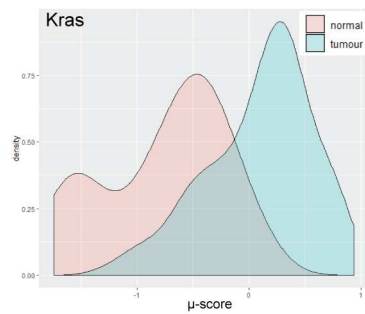
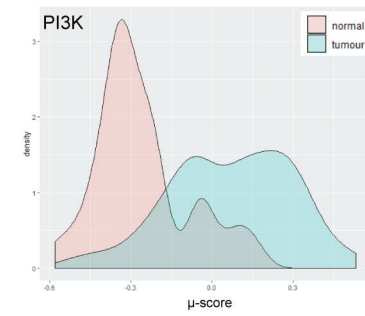
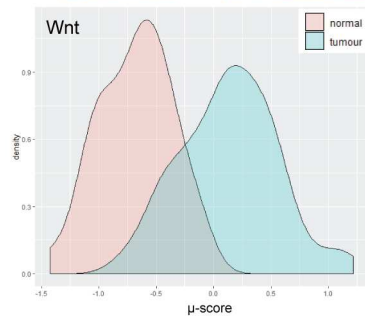
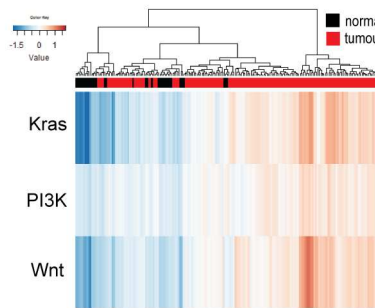
**Extended Data Fig. 6**



## Extended Data Fig. 7

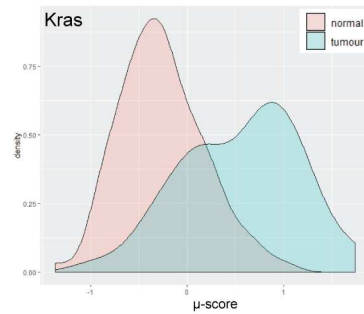
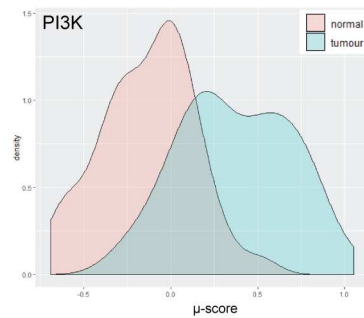
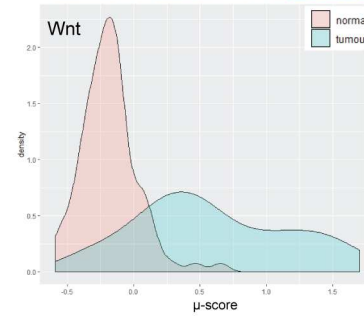
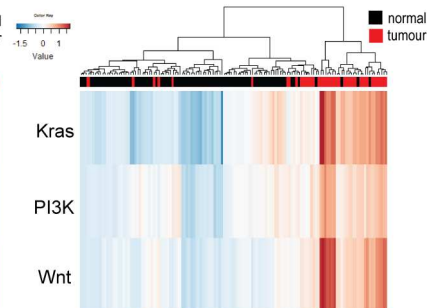
**a** Cancer Genome Atlas  
Research Network (2014)

Hyperactivated pathways	Frequency
Wnt	82.6%
Wnt; PI3K	61.3%
Wnt; PI3K; Kras	59.4%

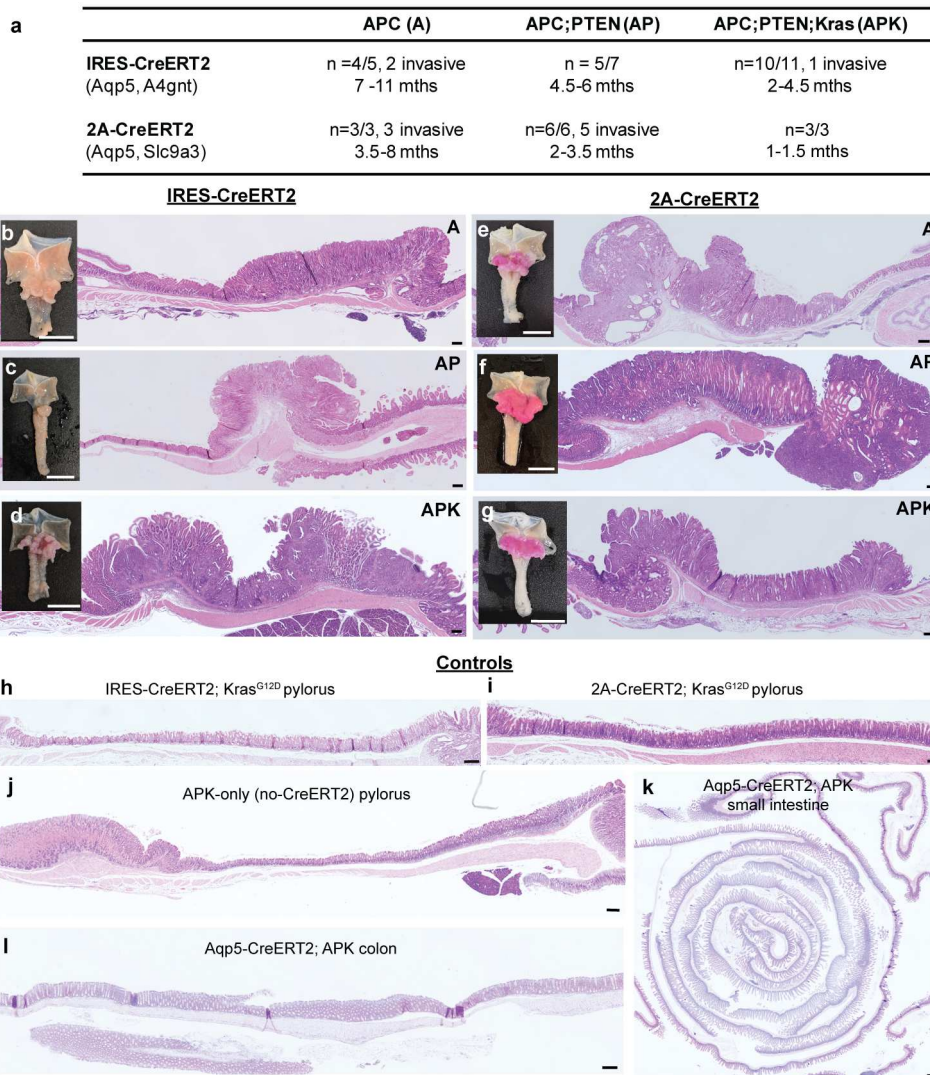


**b** Muratani et al (2014)  
GSE 15459

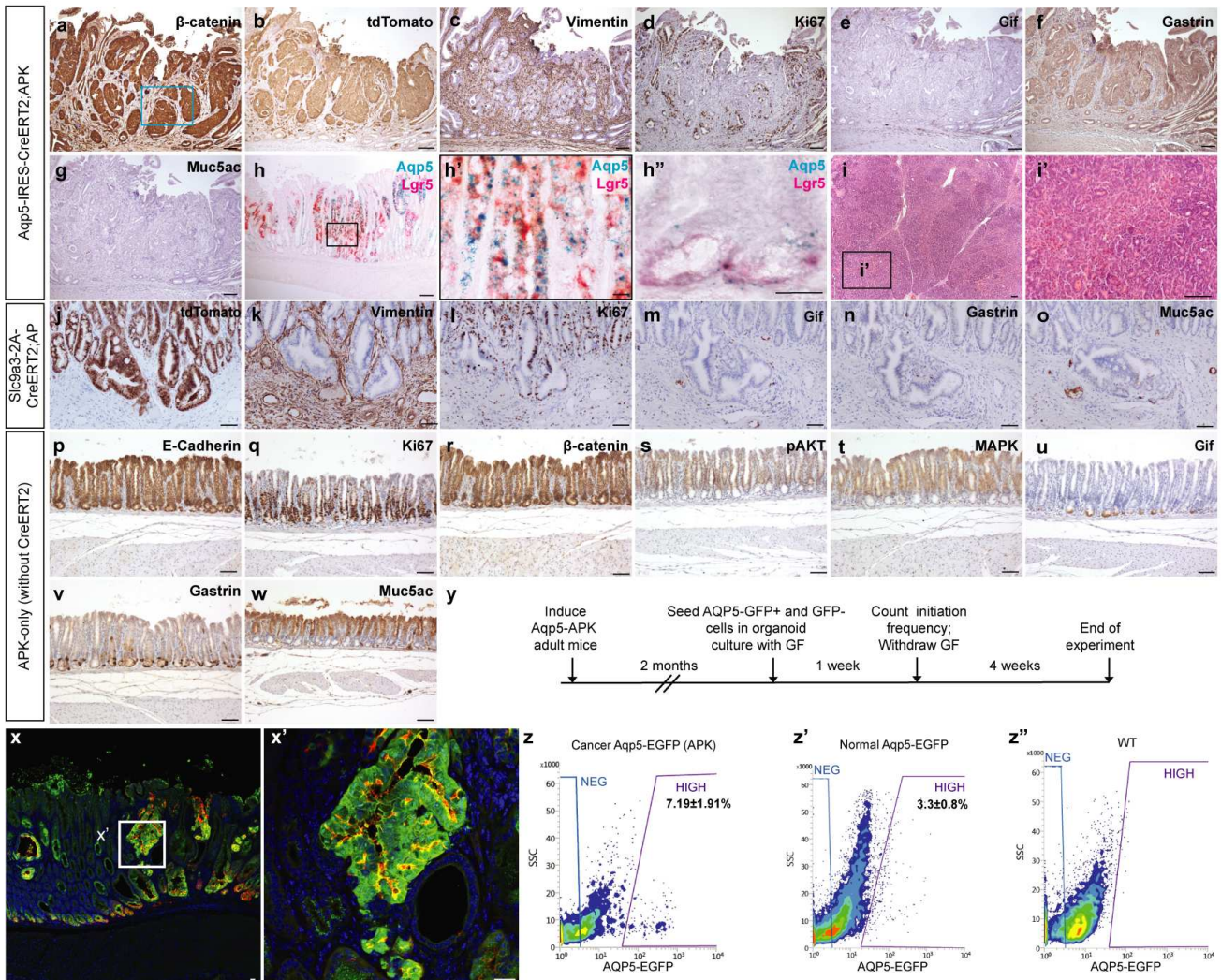
Hyperactivated pathways	Frequency
Wnt	81.0%
Wnt; PI3K	64.3%
Wnt; PI3K; Kras	57.1%



## Extended Data Fig. 8



Extended Data Fig. 9



**Extended Data Fig. 10**

